UNIVERSITY OF CALIFORNIA SAN DIEGO

Novel Machine Learning and Design Methods to Improve EEG-based Motor Imagery Brain-Computer Interfaces

A dissertation submitted in partial satisfaction of the
requirements for the degree
Doctor of Philosophy

in

Electrical Engineering (Machine Learning and Data Science) and Cognitive Science

by

Mahta Mousavi

Committee in charge:

Professor Virginia de Sa, Chair
Professor Vikash Gilja, Co-Chair
Professor Marta Kutas
Professor Scott Makeig
Professor Lawrence Saul
Professor Mohan Trivedi

2019

The dissertation of Mahta Mousavi is approved, and it is acceptable in quality and form for publication on microfilm and electronically:

_____

_____

_____

_____

_____
Co-Chair

_____
Chair

University of California San Diego

2019

DEDICATION

To my parents, for their love and endless support.

TABLE OF CONTENTS

LIST OF FIGURES

LIST OF TABLES

ACKNOWLEDGEMENTS

First and foremost, I would like to express my sincere gratitude to my advisor Professor Virginia de Sa. This dissertation would not have been possible without her support, advice, patience and immense knowledge. I am also thankful to my committee members for their support and constructive feedback in making this dissertation happen.

I would like to thank all my friends in San Diego and across the world. All the hangouts, phone calls and messages have been a great source of support throughout my graduate studies.

I am most grateful to my parents for setting me on the right path. I am where I am now only because of their endless love, support and encouragement. I would also like to thank my sister and brother for all their support, laughter and the wonderful shared childhood memories. Finally, I would like to thank my partner for his love, support and patience, especially in the recent year. I am really thankful and blessed for having so many wonderful people in my life.

I would also like to thank my coauthors and funding sources. My research received support from NSF IIS 1219200, 1817226 and 1528214, NIH 5T32MH020002-18, DAAD short-term research grant, UC San Diego Chancellors Research Innovation Scholarships G2171, G3155 and the Mary Anne Fox dissertation year fellowship.

Chapter 2, in full, is a reprint of material as it appears in Mahta Mousavi and Virginia R. de Sa. "Towards elaborated feedback for training motor imagery brain computer interfaces," Proceedings of the 7th Graz Brain-Computer Interface Conference, Graz, Austria, 2017. The dissertation author was the primary investigator and author of this publication. The copyright for this publication is owned by Verlag der Technischen Universität Graz and used in accordance with their terms and conditions.

Chapter 3, in full, is a reprint of material as it appears in Mahta Mousavi, Adam S. Koerner, Qiong Zhang, Eunho Noh, and Virginia R. de Sa. "Improving motor imagery BCI with user response to feedback," Brain-Computer Interfaces 4, no. 1-2 (2017): 74-86. The dissertation author was the primary investigator and author of this publication. The copyright

for this publication is owned by Brain-Computer Interfaces Journal (Taylor and Francis Group) and used in accordance with their terms and conditions.

Chapter 4, in part, is in preparation for publication as Mahta Mousavi, Laurens R. Krol, and Virginia R. de Sa. "A novel hybrid motor imagery BCI using error-related brain activity," (This is the working title and it may change upon submission). The dissertation author is the primary investigator and author of this manuscript.

Chapter 5, in full, is a reprint of material as it appears in Mahta Mousavi, and Virginia R. de Sa. "Temporally adaptive common spatial patterns with deep convolutional neural networks," 2019 41st Annual International Conference of the IEEE Engineering in Medicine and Biology Society (EMBC), Berlin, Germany, 2019, pp. 4533-4536. The dissertation author was the primary investigator and author of this publication. The copyright for this publication is owned by IEEE and used in accordance with their terms and conditions.

Chapter 6, in full, is a reprint of material as it appears in Mahta Mousavi, and Virginia R. de Sa. "Spatio-temporal analysis of error-related brain activity in active and passive brain-computer interfaces," Brain-Computer Interfaces, in press, (2019). The dissertation author was the primary investigator and author of this publication. The copyright for this publication is owned by Brain-Computer Interfaces Journal (Taylor and Francis Group) and used in accordance with their terms and conditions.

VITA

2019	Ph. D. in Electrical Engineering (Machine Learning and Data Science) and Cognitive Science, University of California, San Diego
2012	M. Sc. in Electrical Engineering, University of Michigan, Ann Arbor
2010	B. Sc. in Electrical Engineering, Sharif University of Technology

PUBLICATIONS

M. Mousavi, and V. R. de Sa,"Spatio-temporal analysis of error-related brain activity in active and passive brain-computer interfaces," *Brain-Computer Interfaces Journal*, 2019, in press.

M. Mousavi, A. S. Koerner, Q. Zhang, E. Noh, and V. R. de Sa,"Improving motor imagery BCI with user response to feedback," *Brain-Computer Interfaces Journal*, 2017.

M. Mousavi, and V. R. de Sa,"Temporally adaptive common spatial patterns with deep convolutional neural networks," *Proceedings of the IEEE Engineering in medicine and biology conference*, 2019.

M. Mousavi, and V. R. de Sa,"Spatio-temporal analysis of feedback-related brain activity in brain-computer interfaces," *Proceedings of the workshop on Modeling and Decision-Making in the Spatiotemporal Domain*, 32nd Conference on Neural Information Processing Systems, 2018.

L. R. Krol, M. Mousavi, V. R. de Sa, and T. O. Zander, "Towards classifier visualisation in 3D source space," *Proceedings of IEEE International Conference on Systems, Man, and Cybernetics*, 2018.

Y. Jin, M. Mousavi, V. R. de Sa, "Adaptive CSP with subspace alignment for subject-to-subject transfer in motor imagery brain-computer interfaces," *Proceedings of the 6th IEEE International Winter Conference on Brain-Computer Interface*, 2018.

M. Mousavi, and V. R. de Sa,"Towards elaborated feedback for training motor imagery brain computer interfaces," *Proceedings of the 7th Graz Brain-Computer Interface Conference*, 2017.

D. Maryanovsky, M. Mousavi, N. Moreno and V. R. de Sa, "CSP-NN: a convolutional neural network implementation of common spatial patterns," *Proceedings of the 7th Graz Brain-Computer Interface Conference*, 2017.

R. K. Maddula, J. Stivers, M. Mousavi, S. Ravindran, V. R. de Sa,"Deep recurrent convolutional neural networks for classifying P300 BCI signals," *Proceedings of the 7th Graz Brain-Computer Interface Conference*, 2017.

M. Mousavi, L. Duan, T. Javidi, A. K. Bowden,"Iterative re-weighted approach to high-resolution optical coherence tomography with narrow-band sources," *Optics Express Journal*, 2016.

M. Mousavi, L. Duan, T. Javidi, A. K. Ellerbee,"Alternative techniques for high-resolution spectral estimation of spectrally encoded endoscopy," *Proceedings of the SPIE Conference*, 2015.

M. Mousavi, K. L. Lurie, J. A. Land, T. Javidi, A. K. Ellerbee,"Telemedicine + OCT: toward design of optimized algorithms for high-quality compressed images," *Proceedings of the SPIE Conference*, 2014.

ABSTRACT OF THE DISSERTATION

Novel Machine Learning and Design Methods to Improve EEG-based Motor Imagery Brain-Computer Interfaces

by

Mahta Mousavi

Doctor of Philosophy in Electrical Engineering (Machine Learning and Data Science) and Cognitive Science

University of California San Diego, 2019

Professor Virginia de Sa, Chair
Professor Vikash Gilja, Co-Chair

Brain-computer interface (BCI) systems read and infer brain activity directly from the brain through for instance electroencephalography (EEG), while bypassing the common neuromuscular pathways. These systems can provide assistive devices for communication and locomotion, interventions for motor restoration and rehabilitation, as well as neurofeedback training for cognitive enhancement. Motor imagery-based BCIs are a category of BCI systems that allow a user to generate control commands by imagining moving different body parts (such as the right or left hand) and the goal of the BCI is to correctly detect the imagined body part from

EEG patterns.

The ability of users to generate discriminable motor imagery-based control signals is very variable and environmental effects such as other brain processes affect current BCI systems to the point that they are mostly limited to lab environments. This dissertation proposes novel machine learning and design methods to improve the performance and reliability of motor imagery EEG-based brain-computer interfaces to provide patients in need, the ability of independent interaction with the outside world. This dissertation proposes: 1) a more elaborate feedback paradigm to allow users to better learn how to generate discriminable motor imagery signal, 2) a novel hybrid motor imagery BCI utilizing the user's brain activity in response to the BCI output (feedback) with improved performance and reliability compared to existing motor imagery BCI systems, 3) an artificial neural network architecture to capture spatio-temporal aspects of the motor imagery signal to improve classification of motor imagery activity, and 4) a novel covariance-based method that uses Riemannian and Euclidean geometry to capture spatial and temporal aspects of the feedback-related brain activity in response to BCI error to further improve hybrid BCIs that utilize this type of brain activity .

By giving improved training feedback and better utilizing the available brain signals, the proposed methods improve the performance and reliability of motor imagery BCIs and provide the chance to greatly increase the number of people who are successfully able to operate one. The developed techniques could also be useful for discovering and training other mental commands that could be used in EEG-based BCIs not limited to motor imagery BCIs.

Chapter 1

Introduction

Brain-computer interface (BCI) systems read and interpret user brain activity directly from the brain bypassing the common neuromuscular pathways [1, 2, 3, 4]. These systems have various applications. For instance, they can provide assistive devices for communication and locomotion [2, 3, 4], interventions for motor restoration and rehabilitation [5], as well as neurofeedback training for cognitive enhancement [6]. However, most existing BCI systems cannot be used independently for daily activities by their intended end users. Poor performance and lack of reliability (i.e. consistency of performance over time) are among major limitations in translating BCI systems from proof-of-concept to everyday application [7].

This dissertation addresses performance and reliability in BCI systems from three different perspectives: 1) by providing richer feedback for improved training of the users enabling better BCI control, 2) a novel BCI design that incorporates the user brain response to the BCI output to further improve the performance and reliability of the BCI, and finally, 3) novel machine learning methods to capture more elaborate features for an improved interaction.

Next, we provide a summary of the major concepts that will be the focus of this dissertation. Then, we describe an overview of the chapters and summarize the significance and contributions resulting from this dissertation.

1.1 Background

1.1.1 Electroencephalography (EEG)

In a BCI system, brain activity is read directly from the brain through invasive or non-invasive techniques [4]. In this dissertation, we focus on electroencephalography (EEG) as it provides a non-invasive, inexpensive and portable intervention to record brain activity with high temporal resolution further facilitating better detection of brain patterns in real-time applications [2, 3]. EEG measures the summation of synchronous electrical activity of thousands or millions of neurons that have similar spatial orientation, through electrodes that are positioned outside of the scalp [4].

1.1.2 Motor imagery

Different types of BCI systems may be distinguished based on the type of EEG pattern the system looks for. One category of BCI systems – motor imagery BCIs – rely on user-initiated movement imagination of different body parts [3]. Imagining different parts of the body results in distinguishable and spatially distinct EEG patterns due to the lateralization and roughly somatotopic organization of the motor cortex [8]. For instance, in a binary motor imagery BCI, a user can imagine movements of her/his right or left hand to control a robotic limb to right or left.

Imagining unilateral hand movements results in the modulation of brain activity in mu (7–13 Hz) and beta (13–30 Hz) bands resulting in an event-related desynchronization (ERD) over the contralateral hemisphere [3].

The motor imagery signal is user-generated. Nevertheless, training users to reliably control their motor imagery signal to interact with a BCI is known to be a difficult task [9]. In this dissertation, we investigated whether providing richer feedback during training allows users to generate a more recognizable motor imagery signal (Chapter 2). We also investigated the spatio-temporal aspects of the motor imagery signal as discussed later in Chapter 5 in order to help

develop an improved motor imagery BCI.

1.1.3 Error-related brain activity

When a user operates a BCI system, the BCI output (feedback) may alter the brain activity and affect the BCI performance. For instance, an erroneous output (feedback) different from the user's intention can result in frustration, loss of control and further distraction. In fact, existing work in the literature shows that the brain activity in response to an erroneous BCI feedback is classifiable [10, 11, 12]. This can therefore be used to improve the BCI performance.

There are various approaches on how to use the error-related brain activity to improve the BCI performance [12]. In one approach, after detecting the error-related brain activity, the last BCI command is discarded and the trial is repeated [11, 13]. The second approach is based on error-driven learning where an adaptive BCI classifier is retrained/recalibrated to limit the BCI from making the same error in the future [14, 15, 16]. A third approach in [17, 18] proposed a hybrid motor imagery BCI with error integration resulting from user brain activity upon change in direction of a cursor in a 1-D cursor control task.

In this dissertation, we proposed a more sophisticated version of the error integration approach by considering motor imagery and error-related brain activity as two different processes. Our approach combines the scores of the motor imagery classifier with the error-related brain activity classifier. This will be explained further in chapters 3 and 4. Later, as discussed in Chapter 6, we investigated the spatio-temporal aspects of the error-related brain activity.

1.2 Dissertation overview

We addressed the poor performance and lack of reliability in EEG-based motor imagery BCI systems through the following studies. We began by investigating a richer feedback during training sessions to allow users to learn better how to control their motor imagery. Then

we investigated the effect of BCI feedback on the motor imagery signal and proposed a novel real-time BCI control that utilizes this information. Finally, we further investigated the spatio-temporal aspects of the motor imagery signal and the error-related brain activity for an improved BCI control.

1.2.1 Chapter 2: Elaborated feedback for training motor imagery BCIs

As mentioned earlier, motor imagery is endogenous and requires extensive training. Therefore, providing relevant and easily interpretable feedback during training sessions is crucial. We proposed an 'elaborated' feedback that provides the users with information pertaining to how they can improve their motor imagery performance. This is in contrast to the conventional training scheme where the user is only informed whether she/he were 'correct'. Our results show that the proposed elaborated feedback methodology allows a better command of the motor imagery signal.

1.2.2 Chapter 3: Investigating feedback-related brain activity in motor imagery BCIs

We designed a study to investigate the effect of feedback-related brain activity in response to BCI error in a motor imagery paradigm. We recorded data from 10 participants performing motor imagery to control a cursor on a screen in front of them. Participants were provided with sham feedback but were led to believe that they were in control of the BCI. This was to have a sufficient number of BCI errors (cursor movements away from the target) for all participants irrespective of their motor imagery performance. We looked at the frequency bands in which the brain response to BCI error is classifiable. We trained a classifier to distinguish if the participant perceived the last cursor movement as good (towards the target) or bad (away from the target). We showed that this good/bad signal is classifiable in similar frequency bands as the

right/left hand motor imagery signal is. Furthermore, we proposed a motor imagery BCI system that uses the good/bad signal as an extra source of information by combining the scores of the right/left hand motor imagery classifier with the good/bad classifier using a logistic regression and showed significant improvement in the BCI performance.

1.2.3 Chapter 4: Improving real-time BCI control using the error-related brain activity

To verify our proposed BCI system in practice, we designed a study to compare our proposed hybrid BCI system with a conventional motor imagery BCI that relies solely on motor imagery brain activity. We recorded data from 12 participants and showed that our proposed BCI system allows participants to perform significantly better. Furthermore, we showed that the good/bad classifier is inherently more reliable than the right/left hand motor imagery classifier. Therefore, the good/bad signal provides a reliable source of information especially in users that do not have a recognizable motor imagery signal.

1.2.4 Chapter 5: Spatio-temporal analysis of the motor imagery signal

Conventional motor imagery classification comprises of two separate phases: a supervised feature extraction phase to train common spatial patterns (CSP) and then a classifier to train on the selected features [19]. A variation of the CSP method, i.e. the filter bank CSP [20], explores temporal aspects of the motor imagery signal by filtering the EEG data into multiple frequency bands before applying CSP in each.

In this chapter, building on our previous work implementing the CSP technique through convolutional neural networks [21], we implemented the filter bank CSP technique through deep convolutional neural networks to capture spatio-temporal aspects of the motor imagery signal in an end-to-end fashion. Our proposed architecture required at most half of the number of

trainable parameters in existing architectures but resulted in similar or improved performance. The reduction in the number of parameters is crucial in noisy data such as EEG for a more reliable classification allowing better generalization.

1.2.5 Chapter 6: Spatio-temporal analysis of the error-related brain activity

Riemannian geometry has been successfully used to classify the motor imagery signal in BCIs [22]. In this chapter, we explored the use of Riemannian methods to better classify the feedback-related brain activity in response to BCI error (i.e., the good/bad signal). We proposed CREST: a novel covariance-based method that uses Riemannian and Euclidean geometry and combines spatial and temporal aspects of the error-related brain activity. Our results show improved performance compared to existing methods in two datasets.

1.3 Significance

BCI systems can provide means of communication as well as autonomous locomotion for patients that suffer from the locked-in syndrome resulting from, for instance, Amyotrophic Lateral Sclerosis (ALS) or brain stem stroke [2, 3, 4]. These systems can also provide rehabilitative interventions for stroke patients [5]. Neurofeedback training is another important application of these systems that can provide cognitive enhancement or help correct some of the brain pattern differences associated with disorders such as autism or attention deficit hyperactivity disorder (ADHD) [6].

As an assistive technology (for communication and locomotion) or as a rehabilitative intervention (post-stroke rehabilitation or neurofeedback training), existing systems rarely leave laboratory environments and are not reliable enough to assist patients in need with their daily activities or to be used for in-home rehabilitation [7]. This highly limits the use of such systems.

When operating a BCI, the user is provided with the BCI output (feedback). The user brain response to the provided feedback can potentially alter the brain signal and result in drifts that make classification of the intended command more difficult. Moreover, since EEG data (time series) is recorded from multiple spatial locations, it has both spatial and temporal aspects. Hence, machine learning methods can provide further insight into better capturing relevant spatio-temporal aspects of the EEG signal to further design more reliable classifiers.

This dissertation addresses various limitations of the existing motor imagery BCI systems through designing a new training scheme, a novel hybrid motor imagery BCI as well as machine learning methods to capture spatio-temporal aspects of the EEG data for improved performance and reliability. Hence, the ideas developed in this dissertation pave the way towards a real solution for patients in need.

1.4 Summary of contributions

This dissertation makes the following contributions to the field of brain-computer interfaces:

1. We proposed a novel motor imagery training protocol comprising of an elaborated feedback which improved the users' control over their motor imagery compared to conventional training methods.

2. We showed that the right/left hand motor imagery signal and the error-related brain activity in response to the BCI feedback occur in similar frequency bands.

3. We proposed a methodology to combine the motor imagery signal and the error-related brain activity in a motor imagery BCI. Our results show significantly improved BCI performance especially in participants who do not have a good motor imagery signal to begin with.

4. We created a modular Python-based real-time motor imagery BCI that will be made open-source for other researchers to use.

5. We demonstrated the efficacy of our proposed method that combines the motor imagery signal and the error-related brain activity, in a real-time BCI control. Our results show significantly improved performance for our proposed method compared to conventional motor imagery control.

6. We showed that the right/left hand motor imagery classifier is more sensitive to the inevitable EEG signal drift compared to the error-related brain activity classifier. Therefore, the latter is more reliable and robust.

7. We proposed a convolutional neural network implementation of the commonly used method of filter bank common spatial patterns to capture spatio-temporal aspects of the motor imagery signal. Our proposed architecture contains at most half of the number of trainable parameters as the existing architectures do while achieving similar or improved performance in two motor imagery datasets.

8. We investigated the use of Riemannian geometry to better classify the error-related brain activity signal.

9. We proposed CREST: a novel covariance-based method that uses Riemannian and Euclidean geometry and combines spatial and temporal aspects of the error-related brain activity in response to BCI output (feedback). We showed improved results on two different datasets: an active motor imagery BCI for 1-D and a passive motor imagery BCI for 2-D cursor control.

Chapter 2

Elaborated feedback for training motor imagery BCIs

2.1 Abstract

Motor imagery is one common paradigm in brain-computer interface (BCI) systems where the user imagines moving a part of his/her body to control a computer. Motor imagery is endogenous and requires a large amount of training for the user to be able to control the BCI. Therefore, the feedback that is provided to the user is critical to ensure informative insight into improving imagery skills. In this study, we investigate a new protocol for providing motor imagery feedback and compare it to the conventional feedback scheme. The proposed feedback focuses on 'elaborating' how the user can improve imagery as opposed to the conventional training protocols which only provide information on whether the user was 'correct' in performing imagery. Our results show that providing more easily interpretable feedback results in more efficient motor imagery training and is preferred by the users.

2.2 Introduction

Brain computer interface (BCI) systems attempt to infer certain cognitive or affective states based on neural signals collected from the brain while bypassing common neuromuscular pathways [2, 23]. One modality to collect brain signals is electroencephalography (EEG) which is popular for being non-invasive and inexpensive. Motor imagery is one common paradigm in EEG-based BCIs in which the user imagines moving a part of her/his body, such as a hand, foot, tongue, etc. Motor imagery of different body parts results in different spatial patterns of decrease in power across the scalp in mu (8–13 Hz) and beta (14–30 Hz) frequency bands [24, 3, 8, 25]. These features are used to distinguish among the imagined classes. One of the advantages of motor imagery based BCIs is that they are endogenous [4]; they do not depend on user response to external stimulation. Endogenous BCIs have several benefits: 1) They do not require the user to have good visual or other sensory responses to respond to exogenous stimuli, 2) They do not require the computer presentation of (possibly annoying or fatiguing) stimuli, and 3) They have the potential to be used in natural asynchronous communication. However, because they are endogenous and depend on the user generating the signal, there are large individual differences in the ability to generate different discriminable motor imagery patterns for different imagined body parts. Therefore, training users to provide classifiable motor imagery signals is critical.

So far, there have been a few training methods proposed in the literature, e.g. [26, 27, 28, 29, 30, 31]. Lotte et al. [9] investigated the current state-of-the-art training approaches and identified flaws in their design based on instructional design literature. They looked at the training approaches at the level of feedback provided to the user, instructions provided to her/him and the task itself. Our current study focuses on the feedback that the user receives. In traditional motor imagery BCI training, the feedback provided to the user is evaluative and corrective, where it only tells the user whether he/she has performed the task correctly and possibly with what confidence [9]. In other words, traditional motor imagery training involves

Table 2.1: The demographics of participants.

Participant ID	Age	Gender	Handedness
P1	18	Female	Right
P2	18	Female	Right
P3	19	Female	Right
P4	21	Female	Right
P5	21	Male	Right
P6	18	Female	Right

giving the user feedback on the output of the classification. When classification is unsuccessful, however, this feedback does not provide any information about why it failed. For example, participants may fail to be successful at right hand vs. left hand motor imagery because they do not induce sufficient mu-desynchronization or the induced desynchronization is bilateral for both right- and left-hand motor imagery.

Motivated by work of [32] we hypothesized that providing richer feedback while users are learning motor imagery would result in faster and better learning. To do so, we decided to provide the users with not just the classification output and its confidence, but a perceivable form of features that are used by the classifier. In other words, our proposed feedback is an example of elaborated feedback as described by [33], where it will provide more easily interpretable feedback and will let users evaluate their performance based on the input to the classifier.

2.3 Methods

We recorded data from 6 healthy participants recruited from the UC San Diego student population. All participants were naive to BCI and motor imagery skills and before participating in the study, signed a consent form that was approved by UC San Diego Institutional Review Board. The demographic details of the participants (i.e., age, gender and handedness) are specified in Table 2.1.

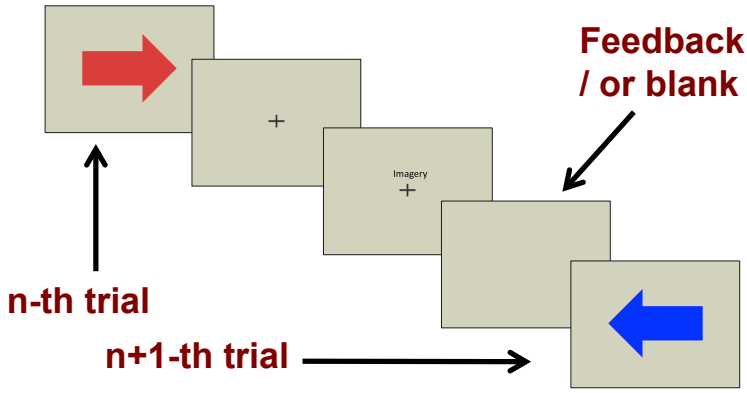

Figure 2.1: An example of a trial in the experiment.

Each participant participated in a one-session experiment consisting of 5 blocks, each consisting of 20 motor imagery trials. Each trial began with an arrow on the screen pointing to the right or the left to specify the trial type. After 1.5 seconds, the arrow disappeared and a cross showed up in the center of the monitor and 1 second later, a term "imagery" on top of the cross appeared. Participants were instructed to begin motor imagery of the corresponding hand (depending on the direction of the arrow) for 3 seconds until the cross disappeared. The participants were instructed to imagine their action of choice so long as it involved a hand movement. Figure 2.1 shows an example of the frames shown in one trial. At the end of each trial in blocks 1, 3 and 5, no feedback was provided. In blocks 2 and 4, the conventional and proposed elaborated feedback were provided which will be described next. Participants 1, 2, and 6 were shown the elaborated and conventional feedback in blocks 2 and 4 respectively. Participants 3, 4, and 5 on the other hand, were presented with the conventional feedback in block 2 and elaborated feedback in block 4. This is to balance the order of the provided feedback types.

We designed our experiment in Python using the Python-based Simulation and Neuroscience Application Platform (SNAP) toolbox [34]. In each trial, data were downsampled to 100 Hz and Laplacian filtered [35] to partially compensate for spatially distributed artifacts by subtracting the mean of the four directly neighboring channels from each channel. Next, an FIR filter of order 225 was used to calculate the average of the power in 3 seconds of motor imagery

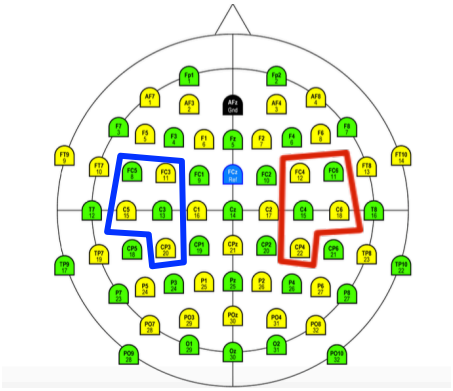

Figure 2.2: Electrode locations in 10–20 international system EEG cap. The selected electrodes were used to calculate power on each side of the motor cortices.

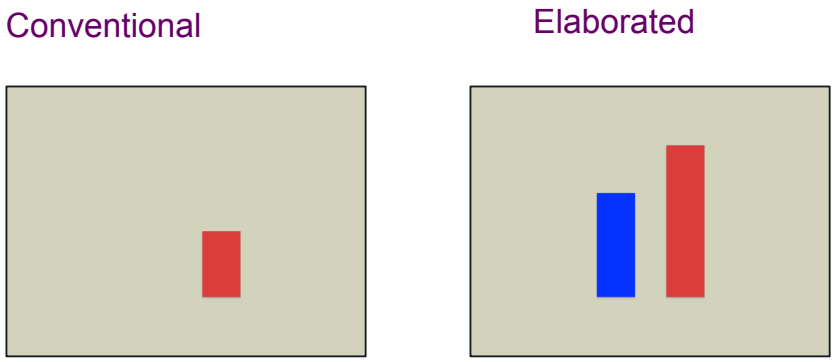

Figure 2.3: Types of feedback.

in the 8–13 Hz frequency band for the channels specified over the right and left motor cortices in Figure 2.2. The average power in each channel was then normalized with respect to the sum of power in all channels specified in Figure 2.2. The conventional feedback was provided as the difference between the power on the two sides and the proposed feedback protocol showed the power on both sides. In each trial, the feedback was provided as a single (static) image after the imagery period was over. Figure 2.3 shows an example of the two types of feedback. Since motor imagery results in contra-lateral de-synchronization of power [8, 25] the participants were instructed to maximize the bar height on the motor imagery side.

As the power over motor cortices may be biased towards one side, we trained a threshold to be the average of the difference in the normalized power on right and left sides of the motor

cortex across trials of each block. In blocks 2 and 4, the threshold that was trained with trials in blocks 1 and 3 respectively, was used to adjust for the potential bias. Therefore, the provided feedback to the participant was based on the adjusted bar heights.

EEG data were recorded with a 64-channel BrainAmp system (Brain Products GmbH) located based on the international 10-20 system, as Figure 2.2 shows. EMG data were also recorded with the same system through two sets of bipolar electrodes on each arm and wrist – for more details on the set-up please refer to [36]. Data were collected with sampling rate of 5000 Hz but were downsampled to 500 Hz for further processing in offline analysis. We chose 500 Hz instead of 100 Hz – which was the rate of the downsampled signal in the online experiment – to keep information in higher frequencies for the purpose of running independent component analysis (ICA) later.

MATLAB [37] and EEGLAB [38] were used for offline analysis. Data were processed in two cases: 1) without artifact removal to investigate the effect of the feedback that was provided to the participants during the experiment, 2) with artifact removal to investigate the effect of training on brain signals and to verify that the participants are not potentially using facial muscle movements to control the bar heights.

In the first case, the raw data were filtered from 8 to 13 Hz with a 500-tap FIR filter. Laplacian filter [35] was applied to partially compensate for spatially distributed artifacts by subtracting the mean of directly neighboring channels from each channel. We looked at the classifier score of each trial in blocks 2 and 4 where the feedback was present. This score is estimated as follows: first the power on each channel over motor cortices is calculated – as shown in Figure 2.2. Then the power on each channel was normalized to the sum of the powers on the specified 10 channels and the average of the power on each side of the motor cortex was used as the classifier score.

We also looked at the classification rates in blocks 1, 3 and 5 where no feedback was provided. To do so, we selected three non-overlapping one-second time windows to cover 3

seconds of imagery period in each trial. Since there are 20 trials in each block, each block has a total of 60 one-second windows of imagery. Next we applied common spatial patterns (CSP) [19] to data from all 64 channels and selected the top 3 filters for each class. Linear discriminant analysis (LDA) [39] was chosen as the classifier to classify right/left imagery classes.

For the second case, we first filtered the raw data using a 500-tap FIR filter in 1 to 200 Hz. Next, we removed up to 6 noisy channels with large muscle artifacts mostly from the temporal and one from the occipital sites. Then the Cleanline EEGLAB plug-in was used to remove the line noise [40]. We removed parts of the EEG data that were suffering from large muscle artifacts; however, no information from the 3 seconds of imagery was removed. We ran independent component analysis (ICA) using the AMICA [41] EEGLAB plug-in to isolate eye and muscle artifacts. Eye and muscle artifacts from the top 30 IC components were removed. Similar analysis to the previous case were performed and the results are described next. Significance in what follows is calculated with a paired-sample two-tailed t-test with 0.05 significance level.

EMG data (4 channels, two on each hand and arm) were bandpass filtered in 10 to 200 Hz using a 500 tap FIR filter, and the line noise was removed with the Cleanline plug-in [40]. EMG data during the three seconds time interval of motor imagery were epoched into nonoverlapping one second intervals and used for classification. Results are presented in the next section.

2.4 Results

To investigate how the right/left classifier score changes over time, we looked at it as a function of the trial number in blocks 2 and 4. For each participant in each trial, the right/left classifier score is calculated as the ratio of the power on the corresponding side as described in the previous section. A line was fit and the slope of the line was estimated. Figure 2.4 shows the slopes calculated in case one (without artifact rejection) as height of the bars in blocks 2 and 4 in

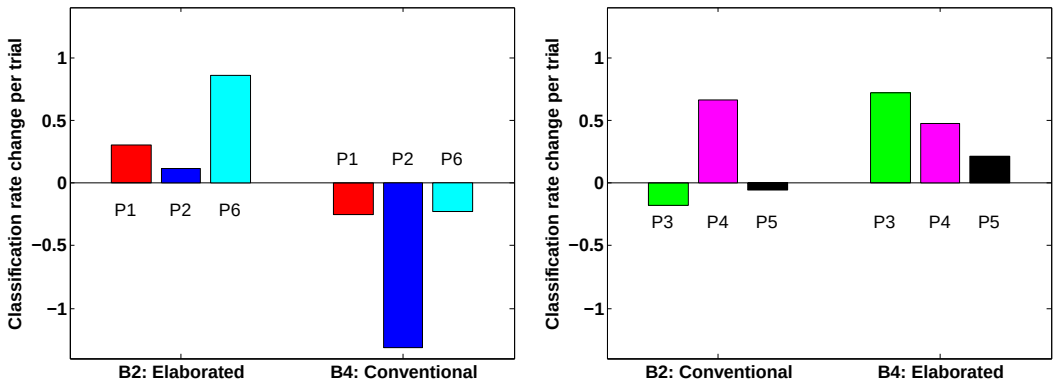

Figure 2.4: Change in percentage points of classification rate per trial in data during feedback blocks, **without** artifact rejection.

separate plots based on whether conventional feedback was provided in block 2 and elaborated in block 4 or vice versa. Figure 2.5 shows the same for data from case two (with artifact rejection). Note that P1, P2 and P6 show some improved performance when the elaborated feedback is provided to them i.e., in block 2. However, they show decreased performance across the trials in block 4 where conventional feedback was provided subsequently. P3 and P5 who were provided with conventional feedback first in block 2, show decreased performance; however, they both show improved performance during the elaborated feedback in block 4. P4 shows improved performance during both feedback types; however, the improvement is higher in the elaborated feedback block when only brain signals are considered, i.e. in Figure 2.5. This shows that the proposed feedback paradigm could potentially be more effective than the conventional feedback.

To verify how the percent change in classification rates per trial (i.e. the height of the bars in Figure 2.4 and Figure 2.5) are different in the two elaborated and conventional feedback conditions among the 6 participants, we ran a paired-sample two-tailed t-test between the bar heights across participants. We found significant difference in both cases with p-values 0.036 and 0.006 for cases one and two respectively – i.e., with and without artifact rejection.

Classification results in no-feedback blocks – 1, 3, and 5 – are provided in Tables 2.2, 2.3,

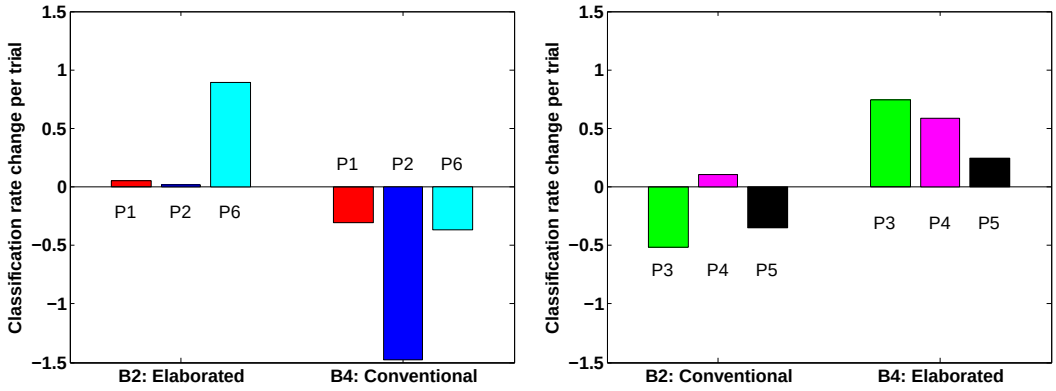

Figure 2.5: Change in percentage points of classification rate per trial in data during feedback blocks, **with** artifact rejection .

Table 2.2: P1, P2, P6 performances **without** artifact rejection

ID	B1	B2	B3	B4	B5
P1	0.58 / 0.048	EF	0.60 / 0.051	CF	0.37 / 0.074
P2	0.73 / 0.051	EF	0.85 / 0.058	CF	0.80 / 0.065
P6	0.75 / 0.057	EF	0.85 / 0.058	CF	0.78 / 0.043

2.4, and 2.5. The training and testing were performed within each block separately and we made sure that both train and test sets were balanced and the test set was absolutely separate from the training. We ran 10-fold cross-validation while making sure that the three one second time windows from one trial will appear all in either train or test sets and the results are presented in Table 2.2 and Table 2.3. For ease of comparison, we have included the type of feedback in blocks 2 and 4 in these tables: EF and CF stand for elaborated feedback and conventional feedback respectively. The first number in each table specifies the mean and the second number is the standard error.

P1, P2 and P6 were provided with the elaborated feedback in block 2. P2 and P6 show improvement in block 3 compared to block 1 which can be associated with the training they received in block 2; however, this improvement is not significant. These two participants also show decreased performance in block 5 which is right after block 4 where they were provided

Table 2.3: P3, P4, P5 performances **without** artifact rejection.

ID	B1	B2	B3	B4	B5
P3	0.52 / 0.080	CF	0.57 / 0.037	EF	0.65 / 0.063
P4	0.82 / 0.072	CF	0.87 / 0.048	EF	1.00 / 0.000
P5	0.42 / 0.057	CF	0.57 / 0.057	EF	0.52 / 0.052

Table 2.4: P1, P2, P6 performances **with** artifact rejection

ID	B1	B2	B3	B4	B5
P1	0.55 / 0.043	EF	0.55 / 0.056	CF	0.47 / 0.060
P2	0.82 / 0.084	EF	0.85 / 0.046	CF	0.85 / 0.052
P6	0.77 / 0.079	EF	0.85 / 0.058	CF	0.83 / 0.043

with the conventional feedback but the decreased performance is not significant. Performance of P1 in all three blocks is below chance level which is calculated as described in [42] to be 62% with significance level of 0.05.

P3, P4 and P5 were provided with conventional feedback in block 2 and elaborated feedback in block 4. P4 shows significant improvement after being exposed to the proposed elaborated feedback in block 4; however, P3 and P5 show chance level performance in all blocks.

To make sure that the classification rates are not affected by non-brain sources including eye and muscle movements, we performed the same analysis described above with the ICA-cleaned data. In this case, we filtered each trial in 8 to 30 Hz frequency band to include both mu (8–13 Hz) and beta (14–30 Hz) frequency bands. The reason we did not include the beta band when we were classifying the non-ICA-cleaned data is that beta band is usually more contaminated with muscle artifacts. After filtering the data, non-overlapping one second time windows

Table 2.5: P3, P4, P5 performances **with** artifact rejection.

ID	B1	B2	B3	B4	B5
P3	0.68 / 0.052	CF	0.52 / 0.052	EF	0.78 / 0.071
P4	0.80 / 0.074	CF	0.82 / 0.063	EF	1.00 / 0.000
P5	0.43 / 0.051	CF	0.55 / 0.043	EF	0.55 / 0.086

Table 2.6: EMG classification results per block.

ID	B1	B2	B3	B4	B5
P1	0.58	0.57	0.52	0.43	0.68
P2	0.32	0.60	0.57	0.55	0.40
P3	0.55	0.47	0.48	0.47	0.48
P4	0.50	0.43	0.82	0.48	0.48
P5	0.58	0.48	0.53	0.62	0.38
P6	0.52	0.33	0.63	0.68	0.57

were selected and 10-fold cross-validation was performed – while making sure that the three one second time windows from one trial will appear all in either the train or test set – to classify right/left motor imagery in blocks 1, 3, and 5 separately. Table 2.4 and Table 2.5 show the classification results. The first number in each table specifies the mean and the second number is the standard error. For ease of comparison, we have included the type of feedback in blocks 2 and 4 in these tables: EF and CF stand for elaborated feedback and conventional feedback, respectively. P3 and P4 who were provided with the conventional feedback first and proposed feedback next, both show significantly improved classification rates in block 5 compared to blocks 1 and 3. Moreover, P3 shows significantly disimproved performance after being exposed to conventional feedback in block 2. On the other hand, P1 and P5 show chance level performance in all of the blocks before and after artifact rejection. P2 and P6 do not show much difference in performance between blocks 3 and 5 after artifact rejection, which was not the case before artifact rejection. It is possible that these participants have been controlling the bars with muscle movements after elaborated feedback not brain signals. Nevertheless, this shows that the elaborated feedback was more effective for the participant to somehow (either through brain signals or muscle) control the bars. Note that since the number of samples in each class is 30, chance level calculated as described in [42] is 62% with significance level of 0.05.

Aside from EEG data, we looked at classification rate of a right/left classifier trained on EMG data in each block. Non-overlapping one second time windows were selected and 10-fold cross-validation was performed while making sure that the three one second time windows from

one trial will appear all in either the train or test set. As Table 2.6 shows, all classification rates are chance level or very close to chance level which is 62% with significance level of 0.05 except for participant 4 in block 3. However, this participant shows improved EEG classification after the elaborated feedback block in which the classification rate on EMG rate is chance level.

2.5 Discussion and conclusion

In this pilot study, we have explored the capability of a visually richer elaborated feedback in training motor imagery BCI and proposed a training protocol that suggests providing the participant the input to the classifier, i.e. an interpretable version of the features that are available to the classification algorithm as opposed to the classifier output. Since any classifier needs data to be trained on and our participants were all naive to motor imagery BCI, we chose to use a very simple classifier, i.e. a threshold, to minimize the effect of instability in a classifier trained with motor imagery data that is changing as the user learns how to control his/her event-related desynchronization signal. All our participants (6/6) chose the elaborated feedback in an answer to a question on the post-study questionnaire: *Which type of feedback did you like better and found more useful?*. This shows that the elaborated feedback approach has the potential to replace the standard conventional feedback paradigm for motor imagery training.

Our results from offline analysis show that the elaborated feedback protocol is potentially more powerful in training motor imagery which is expected as described in [33]. In fact, our participants found the proposed feedback more informative which again emphasizes this point.

One downside of the conventional feedback strategies that our proposed protocol could overcome is the need to have the first block of training with no-feedback or sham feedback as there is no data yet to train a classifier on – the conventional feedback is the output of a classifier. The issue occurs if the participant does not provide proper imagery during this time period, then the classifier is trained on 'incorrect' data. Our method provides the features to the user that

later could be used to train a classifier on. We propose to use the power on the motor imagery cortices and train a threshold to compensate for biases towards either side. Even if the bias is not compensated for, the participant could still be provided with the power on two sides of motor cortices and be instructed to control the bars towards the ideal bar heights, i.e. suppressed power on left side in right hand motor imagery and suppressed power on right side in left hand motor imagery trials. Hence, our proposed elaborated feedback can function without training data.

To evaluate the elaborated feedback further, we are interested in investigating providing participants with the power on both sides of motor cortices normalized with respect to a 'baseline' time period where the participant is relaxed and not performing motor imagery. Another aspect worth investigating further is how the two approaches differ across multiple sessions and to see whether there is more significant difference between the two schemes when more time elapses between training sessions.

2.6 Acknowledgments

This work was supported by the NSF grants IIS 1219200, SMA 1041755, IIS 1528214, and UCSD FISP G2171.

Chapter Acknowledgments

Chapter 2, in full, is a reprint of material as it appears in Mahta Mousavi and Virginia R. de Sa. "Towards elaborated feedback for training motor imagery brain computer interfaces," Proceedings of the 7th Graz Brain-Computer Interface Conference, Graz, Austria, 2017, pages 332-337. The dissertation author was the primary investigator and author of this publication.

Chapter 3

Investigating feedback-related brain activity in motor imagery BCIs

3.1 Abstract

In brain-computer interface (BCI) systems, the non-stationarity of brain signals is known to be a challenge for training robust classifiers as other brain processes produce signals that coincide with those resulting from the desired brain activity. One source of interference is the user's cognitive response to the provided BCI feedback. In the case of motor imagery paradigms, this feedback can for instance be a cursor moving on the screen. The response to such feedback has been shown in general to be a source of noise that can add to the non-stationarity of the brain signal; however, in this work, we show that the users brain response to this feedback can be used to improve the BCI performance. We first show in a motor imagery task that the users brain responds to the direction of cursor movement, which is different for the cursor moving towards or away from the target (i.e. BCI feedback), and this feedback-related information is present in frequency bands similar to those used in motor imagery. Next, we propose a classifier that combines the user response to feedback together with the motor imagery signal itself, and

show that this combined classifier can significantly outperform a conventional motor imagery classifier. Our results show an average of 11% and up to 22% improvement in classification accuracy across 10 participants.

3.2 Introduction

Brain-computer interface (BCI) systems collect and infer neural signals without the use of normal neuromuscular pathways [2, 23, 43, 44]. These systems were originally developed for locked-in patients who suffer from Amyotrophic Lateral Sclerosis (ALS) or brainstem stroke syndrome. Motor imagery (MI) – where a user imagines a movement without producing it – enables effective non-invasive BCI control when measured with EEG [45]. Imagined movements result in an event-related desynchronization (ERD) (decrease in power) in the mu band (8–13 Hz) [8, 25]; a similar ERD occurs in the beta band as well (14–30 Hz) [24, 3]. Motor imagery of different body parts results in somewhat different spatial patterns of desynchronization across the scalp and the BCI uses these features to distinguish among the imagined movement classes. For example, a user might imagine moving their right hand to move a cursor in one direction and imagine moving their left hand to move the cursor in another. The targets can be mapped to different actions to allow a user to interact with the world (e.g. turn a light on or off or move a robot arm to one object or another).

Motor imagery BCIs have an advantage over other non-invasive BCIs as they require neither external stimulation (as needed for steady-state visually evoked potential (SSVEP)[46] and P300-style BCIs [2, 47]), nor gaze control by the user. However, they also have their own challenges, such as their low reliability and information transfer rate, which can confound system use outside a controlled laboratory environment. This low reliability is due in part to the non-stationarity of the brain signals. As these BCIs are not dependent on external stimulation, they rely on signals created internally by the user and are susceptible to contamination from other

brain activity of the user. Due to the low classification accuracies when classification is based on short time windows of EEG recordings containing the motor imagery signal, classification results from several time windows of motor imagery EEG are combined in order to increase the reliability of target selection. The usual method is to use several small time windows of 500-1000 ms and provide feedback in the form of an incremental cursor movement towards the decoded target (for that window) [48]. In this way, the accuracy of hitting the desired target can be boosted at the cost of more time. Improving the classification accuracy in each time step could greatly improve the information transfer rate of the system by reducing the number of steps required to hit the target accurately.

One important factor contributing to contamination of the motor imagery signal is the feedback provided by the BCI itself. It is well understood that BCI feedback is important to help the user learn to perform motor imagery and that providing feedback affects the performance of the user, e.g. [49, 50, 51, 52, 53]. One type of EEG signal that can be generated in response to feedback is the error-related potential (ErrP), which can help distinguish between movements in the desired direction and those in the non-desired direction [12]. Schalk et al. [10] reported that in an EEG-based cursor control BCI through modulation of mu and beta rhythms, participants elicited error-related potentials at the end of erroneous trials. Ferrez and Millan in [54] reported detection of error-related potentials in an experiment where the participants manually controlled the cursor movement. In another study [11], they showed the application of the detected error-related potential in improving the classification rate of a motor imagery task by undoing movements associated with detected error-related potentials. Artusi et al. [55] proposed a strategy of repeating trials when an error potential is detected. Authors in [13] and [56] improved performance of speller BCIs by correcting for the detected error from user feedback. Detection of errors for adaptably calibrating a code-modulated visual evoked potential (c-VEP) classifier was proposed in a c-VEP BCI [16]. Kreilinger et al. [57] showed the classifiability of error-related potentials during continuous movement of an artificial arm provided as delayed feedback in a

right-hand motor imagery task. Koerner [17, 18, 51] investigated methods to classify and use error-related potentials while the participant was performing motor imagery. Omedes et al. [58] investigated error-related potentials in the frequency domain but only in the lower frequencies (theta band, 4-8 Hz). In an electrocorticographic (ECoG) BCI study, Milekovic et al. [59] found error-related neural responses in lower-frequency bands similar to ErrP studies in EEG as well as high gamma (beyond 60 Hz) carrying partially independent information. However, high gamma information is difficult to obtain from EEG data.

The error-related potentials (ErrP) mentioned above are temporal signals usually observed in EEG signals filtered between approximately 1 and 10 (or sometimes up to 20) Hz [54, 58, 60]. In this study, we investigate the response to visual feedback of motor imagery while the user is actively performing motor imagery. Our goal is to look for error-related information in other frequency bands (not just low-frequency traditional error-related potentials) and in other spatial locations (not just on the center midline channels). We introduce the term error-related spectral perturbation (ErrSP) as a certain type of event-related spectral perturbation [61] to emphasize that we look beyond error-related potentials (ErrP), i.e. in multiple frequency bands and in a data-driven manner in the spatial domain.

We show that the polarity of the feedback (whether the cursor moves in the direction the user intended or in the opposite direction) is classifiable and that some of the information used for classification is contained within the same frequency bands that are important for motor imagery. We then present a method to make use of the classifiability of the brain response to such feedback. The idea is to combine the active motor imagery that the user is generating along with the passive response [62, 63] to the cursor movements to best determine the desired cursor movement direction/target location. Our results show that the proposed approach significantly outperforms the conventional approach in motor imagery.

Table 3.1: Demographics of participants.

Participant	Age	Gender	Handedness
One	20	female	left-handed
Two	18	male	right-handed
Three	19	female	right-handed
Four	22	male	right-handed
Five	19	male	left-handed
Six	18	female	right-handed
Seven	25	female	right-handed
Eight	34	male	right-handed
Nine	22	female	right-handed
Ten	19	male	right-handed

3.3 Methods

3.3.1 Paradigm

We collected data from 10 participants who were recruited from the UC San Diego student population after the study was approved by the University Institutional Review Board. The demographic details are specified in Table 3.1 as age, gender and handedness for each participant.

Participants were naive to BCI and signed a consent form approved by the UCSD Human Research Protections Program before participating in the experiment. The experiment consisted of two parts: in phase one, the participants were trained to perform kinesthetic motor imagery of left and right hands. It has been shown previously that kinesthetic motor imagery (imagine what it feels like to move your hand) induces a stronger EEG signal [64] than visual motor imagery (imagine what your hand moving looks like). This phase consisted of a total of 30 trials, divided into 3 blocks of 10 trials each. Each trial began by randomly showing an arrow pointing to the left or right to indicate the trial being a left- or right-hand motor-imagery trial respectively. Then a cross appeared at the center of the screen, and after one second the phrase motor imagery

appeared on top of the cross. Participants were instructed to perform kinesthetic motor imagery as long as the cross and motor imagery phrase were on the screen (i.e. for 4 s). At the end of this time period, participants were provided with true feedback in terms of two bars, whose height reflected the average power in the mu band (8–13 Hz) of small Laplacian-filtered [35] signals from channels over the left (C3, FC3) and right (C4, FC4) motor and pre-motor cortices [8]. Participants were instructed that they should aim for maximizing the difference between the height of the two bars, with the higher being on the side of the imagery target. For instance, on a right imagery trial, the bar on the right side should have a greater height than the one on the left and this difference should be as large as possible (though the participants were not informed of the reason, this is because the desynchronization - decrease in power - is greater on the side contra-lateral to the imagined body part). The powers of the two bars were scaled if the larger power was greater than a threshold so that the bar heights were visualizable on the monitor. The bars were presented on the screen for 2 s and the inter-trial interval was set to about 10 s - a random duration between 0 and 1 s was added to the rest period to prevent adaptation. Phase 1 was designed to be a short training session to give participants the chance to learn how to perform discriminable motor imagery during phase 2. Phase 2, which will be described next, is the main part of the experiment; all analysis and the reported results are from data collected during this phase.

In phase 2, participants were instructed to use motor imagery to move a cursor on a horizontal line on the monitor to hit a target on the left or right. This paradigm is an extension to what was originally proposed in [18, 51]. Each trial began by showing the cursor in the center of the screen and the target at either end on the right or left side. The cursor and target were each represented as a circle having 2 cm diameter, and colored blue and white respectively. The center position (where the cursor would begin moving from) was three steps away from both right and left sides where the target would appear. After 1.5 s the target vanished to reduce visual distraction for participants and ensure that classification was not based on a visual signal. The cursor

moved every 1 s based on a pre-determined sequence of movements. Each trial ended when the cursor hit the target position (success) or the other end of the screen (failure). An example of the paradigm is presented in Figure 3.1-left. There were 10 blocks in this phase, each composed of 20 trials. Participants performance within the past block and the overall performance were provided on the screen after each block. Participants were misled to believe they were controlling the cursor while in fact sham feedback was used to keep the stimuli consistent among them. Participants were told that performances above a certain level would be rewarded monetarily (over the regular compensation). During the rest period in between the trials, the participants kept their eyes open but did not fixate on the center of the monitor. They could look around and blink normally. During the rest period in between blocks, the participants had as much time as they wanted to relax and stretch out and close their eyes and take some rest.

As mentioned earlier, the cursor followed a pre-determined pattern which was determined pseudo-randomly with a few conditions enforced: target hit rate for the blocks varied between 60 and 90%; in each trial from the cursor beginning in the center until the end at most three changes in direction were allowed; no more than two consecutive changes in direction were possible; and finally, the cursor started in the middle of the screen and ended at the right or left side of the monitor (not in other locations). The sequence of trials and the cursor movement pattern were kept the same for all participants and was designed to have an adequate number of cursor movements towards and away from the target.

3.3.2 Data collection and processing

Data were collected with a 64-channel BrainAmp system (Brain Products GmbH), with electrodes arranged according to the International 10–20 system [65]. The impedance of the electrode connectivity was adjusted to be below 6 kΩ. Aside from EEG data, EMG data were recorded with the same system through bipolar electrodes, one on the upper forearm and another on the wrist of each hand, as shown in Figure 3.1-right. Both EEG and EMG data were collected

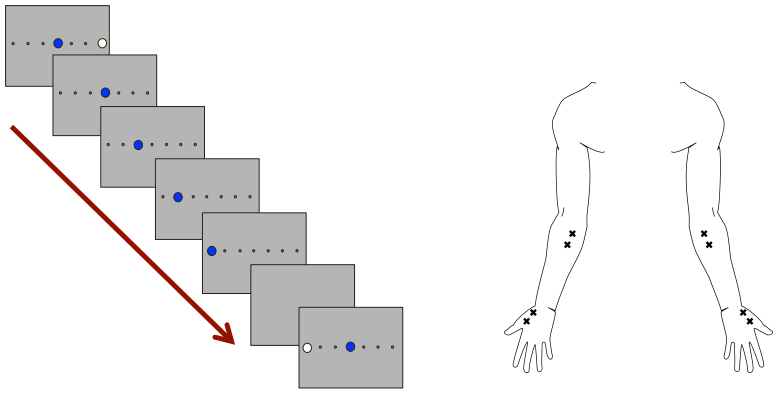

Figure 3.1: Left: one trial of the paradigm in the second (main) phase of the experiment. The participants were instructed to move the cursor to the target with motor imagery of their left or right hands. Right: bipolar electrode placements on each arm.

at 5000 Hz sampling rate and downsampled to 500 Hz for further processing.

Pre-processing was done in MATLAB [37] and EEGLAB [38]. Data were first band-pass filtered between 1 and 200 Hz with an FIR filter with 500 taps and the Cleanline plug-in [40] was applied to remove the line noise. Data sections contaminated with large muscle artifacts were identified visually and removed. The rejected sections contained less than 5% of the data recorded during trials. Next, one to five channels with high power in the higher frequencies (above 60 Hz), indicating channels possibly contaminated by muscle or other artifacts, were removed. All these channels were from electrodes over temporal sites. Then, the EEG data were epoched into 500 ms non-overlapping intervals and automatic artifact rejection – `autorej` and `jointprob` – from EEGLAB was applied to remove at most 10% of the data. Then Infomax ICA decomposition [66] was applied and ICA components were saved. Afterwards, the raw data were once more band-pass filtered between 0.1 and 50 Hz, and the data sections contaminated by large muscle artifacts were visually identified and removed. No epoching or automatic artifact rejection was performed in this round and only ICA components that were saved earlier were applied to remove muscle and eye artifacts based on the instructions in [38].

3.3.3 Classification

Data were band-pass filtered with an FIR filter with 500 taps in the following frequency intervals: 1–3, 2–5, 4–7, 6–10, 7–12, 10–15, 12–19, 18–25, 19–30, 25–35, and 30–40 Hz. These intervals were selected to cover low and high theta, mu, and beta frequency bands while overlapping to compensate for individual differences [67, 20]. The pre-processed data were epoched 150 to 950 ms after each cursor movement. The notion of *step* in the rest of the paper represents this time window after each cursor movement and classification is explored at this level. This interval was selected to take into account the time that it took for the participant to perceive the cursor movement. Note that in general for reporting BCI performance, it is standard to consider all time intervals in the course of cursor sequence/trial, beginning in the middle of the screen and ending at either side (right or left), and to compute accuracy on this scale in terms of the hit-rate for hitting the correct target. However, as our goal is to look for the user response to feedback in short-time recordings of EEG while the user is performing motor imagery, we compute accuracy on a single *step* basis (only the time periods between two consecutive cursor movements).

Common spatial patterns (CSP) were applied to extract the top three filters for each class and in each frequency band [19]. After applying the trained CSP filters, features were extracted as the log of the power through each filter for each step. Other than log power in the aforementioned frequency bands, different features were also extracted from the temporal signal (single-step version of the event-related potential [ERP]). The pre-processed data were bandpass filtered from 0.5 to 10 Hz, with an FIR filter comprising 500 taps. Signals in each channel were averaged in non-overlapping 50 ms windows from 150 ms to 950 ms in the time domain and these values from channels Cz, Pz, CPz, and Fz were selected as ERP features.

Each step, that is each cursor movement, depending on the location of the target (either on the right or left) and the movement (towards [good] or away from the target [bad]), can be divided into four categories: good-right (GR), good-left (GL), bad-right (BR), and bad-left (BL). Classification in all cases described next, was done on balanced classes, i.e. the number of

steps in GR, BR, GL, and BL classes were balanced by randomly removing steps from classes with a higher number of steps. Linear discriminant analysis (LDA) classification [39, 68] was performed over each cursor movement with two different classifiers: one being the conventional right/left (R/L) classification to classify the motor imagery signal, and the other classifying the 'goodness' of each cursor movement, i.e. to decide whether the cursor moved toward the target - good movement = or away from the target - bad movement. We call the latter a good/bad (G/B) classifier (in contrast to the standard R/L). Since we looked into two different sets of features for the G/B classifier, i.e. power and ERP features, we name the two G/B-p and G/B-erp accordingly. We present classification results for R/L, G/B-p, and G/B-erp classifiers separately, as well as for combinations of these classifiers, as discussed next.

Our first attempt to combine the two R/L and G/B-p classifiers is within each frequency band (per-frequency-band classifier). For each step, the probabilities of belonging to the right class and good class are considered as scores from the R/L and G/B-p classifiers respectively. However, to combine the two output features consistently in one classifier, the direction of the observed cursor movement must be taken into account to allow translation of the G/B outputs into the R/L output space, since the output of the combined classifier is to determine the motor imagery intention. If the cursor moved to the right, then the movement was a GR or BL. Therefore, the G/B-p classifier maps to R/L space; hence, the probability of belonging to the good class is the same as the probability of belonging to the right class. On the other hand, if the cursor moved to left, the movement was either GL or BR. In this case, the G/B-p classifier maps to L/R as opposed to R/L. Therefore, the probability of being in the good class is the same as the probability of being in the left class; hence, the G/B score is translated by one minus the probability of belonging to the good class. We call this process translation of features based on the observed cursor direction of movement. After translation, R/L and G/B-p classifier scores were combined through logistic regression.

We also propose a combined R/L and a combined G/B-p classifier that both use the

features across all frequency bands (across-frequency-bands classifiers). These classifiers train a logistic regression over the scores from frequency bands that show R/L or G/B-p classification rates above chance level with respect to the number of steps with significance level of 0.01 [42, 67]]. Note that the test data (steps) remained unseen during the training session, including the logistic regression part. To see whether dividing the signal into many frequency bands is more effective for discriminating R/L motor imagery than using one classifier over one 7–30 Hz frequency band, we compare the performance of the combined across-frequency-bands R/L classifier with that of a conventional R/L classifier that trains an LDA classifier on the log power features from the top three CSP filters for each class in one 7–30 Hz frequency band.

To make use of the responses to the 'goodness' of cursor movement, we propose to augment the R/L across-frequency-bands classifier to a [R/L]+[G/B-p] across-frequency-bands classifier that uses motor imagery information as well as the state of the participant with respect to each cursor movement in relevant frequency bands. For each participant, this classifier selects LDA features in terms of probabilities of belonging to each class, based on frequency bands with significantly above chance R/L or G/B-p classification rates. The chance level was calculated based on the number of steps with significance level of 0.01 [42, 67]. A logistic regression classifier was trained over LDA scores from the selected R/L and G/B-p frequency bands. Translation of G/B-p scores (probabilities) into R/L was performed based on the observed cursor direction of movement as described earlier. We compare this with across-frequency-bands [R/L]+[G/B-erp] classifier that uses ERP features instead of power features in a similar way. Translation of G/B-erp scores to R/L was performed in the same way as translation of G/B-p scores to R/L, as explained earlier.

The ultimate proposed classifier is one that uses all sets of available features described earlier. Therefore, we propose a combined across-frequency-bands [R/L]+[G/Bp]+[G/B-erp] classifier that uses motor imagery information as well as the state of the participant with respect to each cursor movement in both frequency (G/B-p) and time (G/B-erp) domains. Similar to the

[R/L]+[G/B-p] classifier, the frequency bands in which R/L and G/B-p perform above chance level with respect to the number of steps with significance level of 0.01 [42, 67] were selected. LDA scores for the G/B-erp classifier were concatenated to the selected G/B-p scores, while translated to R/L based on the observed cursor direction of movement as described earlier. A logistic regression classifier was trained over all three sets of scores: R/L as well as translated G/B-p and G/B-erp. As before, the test data (steps) remained unseen during both parts of training the classifier.

EMG data were collected to confirm that classifying right-left motor imagery is not possible from arm/wrist movements. Data from the bipolar channels on the forearm and wrist on each hand were bandpass filtered from 10 to 100 Hz with an FIR filter with 500 taps. The line noise was removed with the Cleanline plug-in [40] in EEGLAB [38]. Data were epoched 0 ms to 1000 ms after each cursor movement and the log power of the signal was used as the feature for classification in a separate control classifier using LDA.

In all of the results reported next, we made sure that train and test steps (beginning from the feature extraction phase) were absolutely separate subsets of steps and performed multiple 10-fold nested cross validations for all classification results.

3.4 Results

Table 3.2 compares the classification results for the combined-across-the-frequency bands R/L classifier that uses classifier scores trained on several different frequency bands and the conventional R/L classifier trained on features over one 7–30 Hz band. A paired-sample two-tailed t-test shows that the R/L classifier combined across multiple frequency bands performs significantly better for participants 4, 6, and 8. For the rest of the participants, the performance is not significantly different. We decided to continue using the combined-across-the-frequency-bands R/L classifier as later on we are interested in looking at both R/L and G/B classifiers in

multiple frequency bands including lower than alpha frequencies. Note that the classification rates that are reported here are after each cursor movement within a time window of length 800 ms.

To make sure that the results presented here are due to motor imagery and not actual movement execution, we performed R/L classification on EMG data as well. Table 3.2 also shows the results for the R/L classifier on EMG data for each participant and the class conditional correlation with the combined-across-the-frequency-bands R/L classifier on EEG data. To do so, we first corrected for different means between the right and left classes in each case and then calculated the correlation coefficient and the corresponding p-value for each participant. As Table 3.2 presents, participants 2 and 4 show significant correlation between R/L classifiers trained on EEG and EMG data; however, the correlation coefficient for participant 4 is very small and the R/L classification rate on EMG data for participant 2 is only chance level. Therefore, we conclude that the classification rates reported for R/L classifier on EEG data are in fact from motor imagery and not actual movements. To be consistent, we also trained a G/B classifier on EMG recordings and found chance-level performance for all participants.

Figure 3.2 shows the results of LDA classification for R/L and G/B-p in each frequency band; i.e. the solid and dashed black lines. The magenta line shows the combined-per-frequency-band R/L and G/B-p classifiers in each frequency band separately. Each point on the plots is represented as an error bar showing the mean and standard error of results from five instances of 10-fold cross validation. The dashed green line represents the chance level 0.5 and the solid green line indicates the chance level calculated based on the number of steps [42] with significance level of 0.05. As can be noted from the plots, the combined classifier outperforms the R/L classifier in frequency bands where G/B-p performs above chance level.

Note that, for all participants, lower-frequency bands (below 10 Hz) show above-chance-level G/B-p classification performance. We hypothesized that this might be reflecting error-related signals that might be better classified using a conventional windowed-mean classifier on

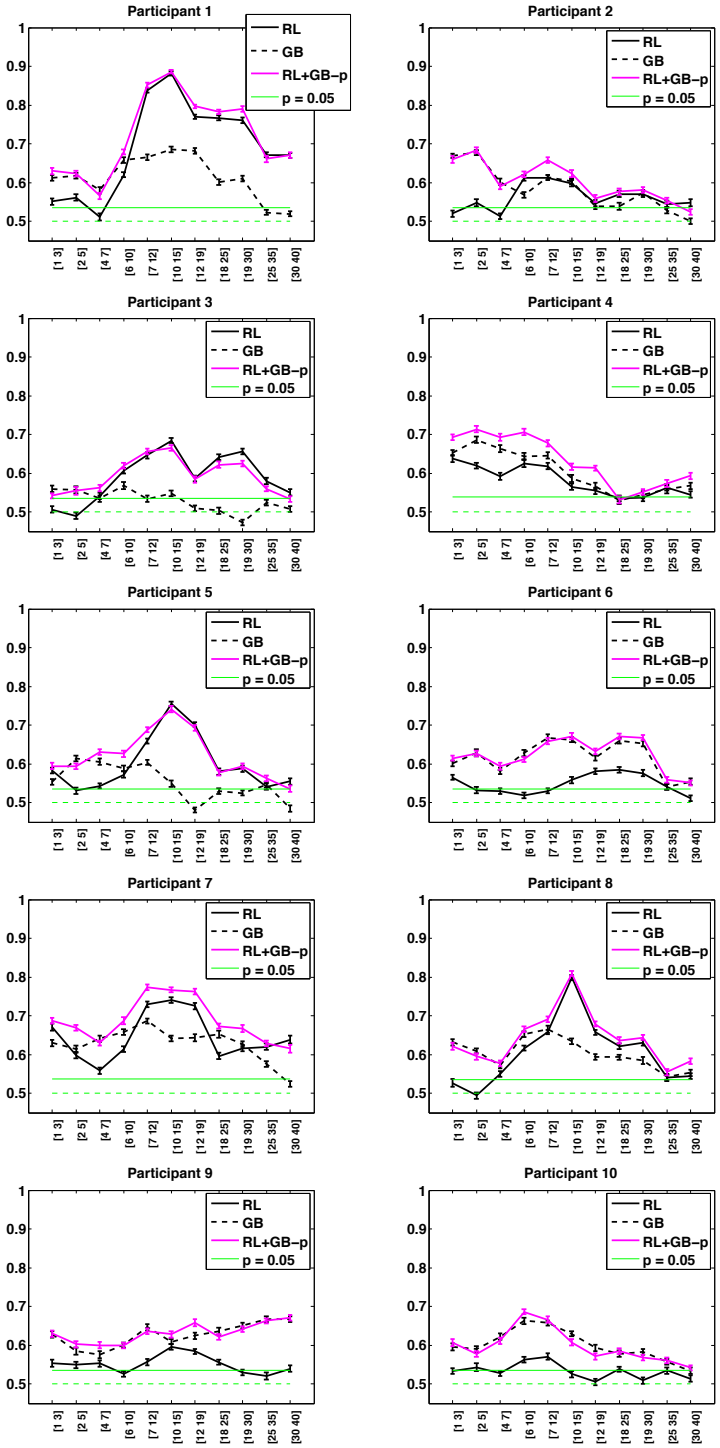

Figure 3.2: The black solid and dashed lines show the result of LDA classifiers on R/L and G/B-p respectively, trained on the individual frequency bands. The magenta line is the combined R/L and G/B-p classifier per frequency band.

Table 3.2: Comparison of conventional R/L classifier (7–30 Hz R/L) and the combined across-frequency-bands R/L classifier. The first number is the mean classification rate over five instances of 10-fold nested cross validation and the second number is standard error. The significantly higher rates among the two are identified in bold. The fourth column presents the R/L classifier results on EMG data with mean and standard error over five instances of 10-fold cross validation. The last two columns show the correlation coefficient and corresponding p-value between the combined across-the-frequency-bands R/L classifier on EEG data and the R/L classifier on EMG data.

Participant	R/L	7-30 Hz R/L	EMG	corrcoef	p value
One	0.87 / 0.005	0.86 / 0.005	0.63 / 0.008	0.008	0.719
Two	0.60 / 0.010	0.61 / 0.006	0.54 / 0.008	0.17	$<$0.01
Three	0.68 / 0.012	0.66 / 0.007	0.55 / 0.010	0.039	0.069
Four	**0.68 / 0.010**	0.63 / 0.009	0.63 / 0.007	0.080	$<$0.01
Five	0.73 / 0.010	0.74 / 0.007	0.50 / 0.009	-0.032	0.277
Six	**0.63 / 0.012**	0.56 / 0.008	0.55 / 0.007	0.029	0.170
Seven	0.78 / 0.009	0.77 / 0.007	0.61 / 0.009	-0.016	0.466
Eight	**0.79 / 0.010**	0.74 / 0.007	0.56 / 0.008	-0.018	0.390
Nine	0.60 / 0.011	0.60 / 0.008	0.53 / 0.008	-0.026	0.379
Ten	0.57 / 0.010	0.56 / 0.008	0.56 / 0.007	-0.001	0.957

the low-pass-filtered temporal signal. In order to investigate whether G/B-p classifiers and G/B-erp classifiers are classifying different signals in both lower and higher frequency ranges, we looked at the class conditional correlation coefficients between the real-valued classifier outputs of the G/B-p and the G/B-erp classifiers. We did this separately for the good and bad classes to exclude significant correlation that may result when both classifiers perform above chance. We calculated the correlation coefficient between the LDA scores computed based on each classifier in each step. Our results show that there are no significant correlations in higher-frequency bands except for participants 6 and 10, though they are fairly low valued – R below 0.15. This implies that in fact G/B-p (when performing above chance level) is using new information which is not considered by G/B-erp in the 0.5–10 Hz frequency band. In fact the correlations between G/B-p and G/B-erp are small (and for some participants not significant) even in the lower frequencies. Thus we decided to keep all G/B-p features as well as the G/B-erp features in our proposed

classifier [R/L]+[G/B-p]+[G/B-erp].

We introduce the term error-related spectral perturbation (ErrSP) for CSP-filtered EEG data and calculated it for each participant: see Figures 3.3 and 3.4. In each frequency band, we ran 10-fold cross validation and found the top three CSP filters in each class for G/B classification in each fold. Next LDA was trained on the log-power of the CSP-filtered train data, and the LDA-weighted log power of CSP-filtered test data in each fold in 50 ms non-overlapping time windows was calculated. A paired-sample two-tailed t-test was run to measure the significance of the difference in good (G) and bad (B) classes in each time window and each frequency band. P-values are also plotted in Figures 3.3 and 3.4. These results show that there is classifiable information beyond the low-frequency ErrP on center-line channels which could be used in better detecting the polarity of feedback, i.e. whether the cursor is moving towards or away from the target.

Table 3.3 shows classification results for G/B-p and G/B-erp and [G/B-p]+[G/B-erp] classifiers. For each we ran paired-sample two-tailed t-tests between G/B-p and [G/B-p]+[G/B-erp] and another test between G/B-erp and [G/B-p]+[G/B-erp]. Whenever [G/B-p]+[G/B-erp] results in significantly higher performance compared to both G/B-p and G/B-erp, the result is specified in bold. Note that for all participants except for participant 3, the combined classifier performs significantly better than either of the two pieces of information separately (with significance level of 0.05). Moreover, all participants except for 3, 4, and 8 show significantly improved combined classifier with significance level 0.01.

Table 3.4 presents the results for the R/L, [R/L]+[G/B-p], [R/L]+[G/B-erp], and [R/L]+[G/B-p]+[G/B-erp] classifiers when information across all frequency bands is taken into account. The first number is the mean classification rate with three instances of 10-fold nested cross validation and the second number shows the standard error. Paired-sample two-tailed t-tests were calculated for the proposed [R/L]+[G/B-p]+[G/B-erp] classifier, i.e. the last column in Table 3.4, in comparison with the R/L classifier, i.e. the second column in the same table, and if the

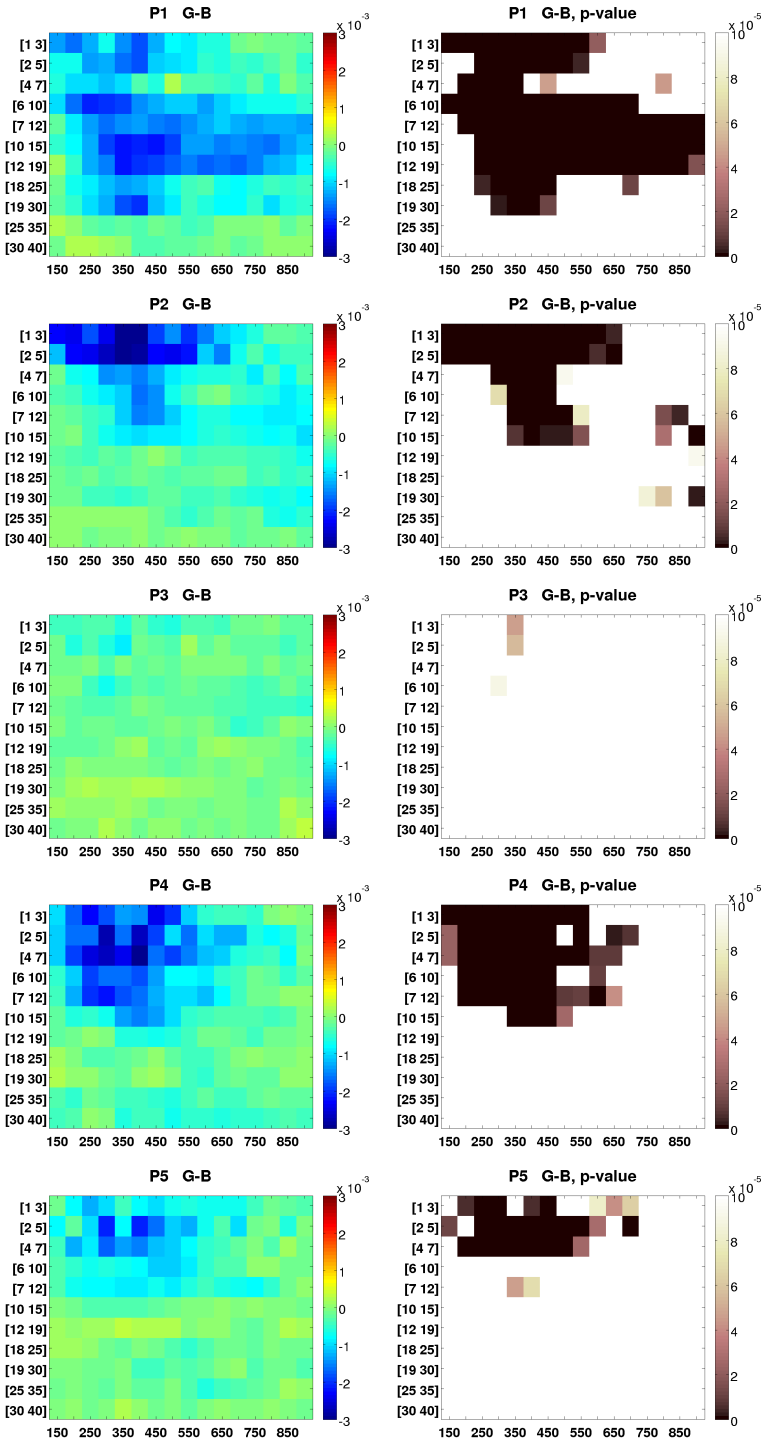

Figure 3.3: ErrSP (left column) for G-B difference and p-values from paired-sample two-tailed t-tests between good and bad classes in participants 1-5 in various frequency bands/time bins. X-axis shows the time in ms after cursor movement and Y-axis the frequency bands. P-values are uncorrected but are only shown for p-values $< 10^{-}4$.

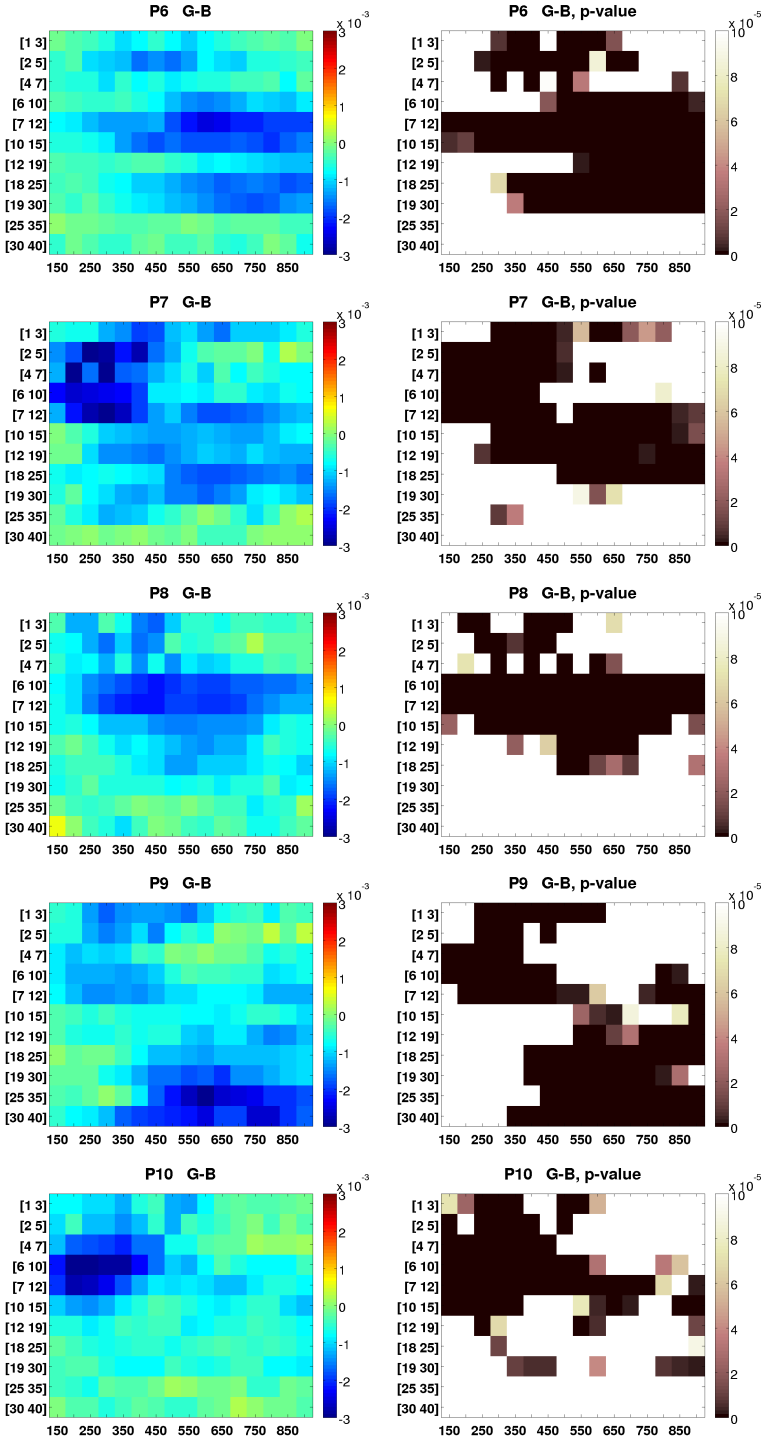

Figure 3.4: ErrSP (left column) for G-B difference and p-values from paired-sample two-tailed t-tests between good and bad classes in participants 6-10 in various frequency bands/time bins. X-axis shows the time in ms after cursor movement and Y-axis the frequency bands. P-values are uncorrected but are only shown for p-values $< 10^{-}4$.

Table 3.3: Comparison of G/B-erp and G/B-p classification rates. The last column shows the results of the combined classifier. The first number is the mean classification rate over three instances of 10-fold nested cross validation and the second number is the standard error. Whenever the combined classification rate is significantly higher than both G/B-p and G/B-erp, the number is specified in bold.

Participant	G/B-p	G/B-erp	G/B-p+G/B-erp
One	0.76 / 0.010	0.73 / 0.007	**0.81 / 0.007**
Two	0.73 / 0.010	0.73 / 0.008	**0.77 / 0.009**
Three	0.54 / 0.009	0.60 / 0.009	0.59 / 0.010
Four	0.74 / 0.010	0.78 / 0.006	**0.81 / 0.011**
Five	0.65 / 0.009	0.66 / 0.008	**0.71 / 0.007**
Six	0.71 / 0.009	0.69 / 0.007	**0.75 / 0.009**
Seven	0.75 / 0.009	0.72 / 0.010	**0.79 / 0.007**
Eight	0.67 / 0.012	0.72 / 0.008	**0.75 / 0.010**
Nine	0.76 / 0.009	0.75 / 0.009	**0.81 / 0.008**
Ten	0.70 / 0.012	0.70 / 0.007	**0.76 / 0.009**

difference is significant (with 0.01 significance level) the higher rate is identified in bold. We ran paired-sample two-tailed t-tests with 0.01 significance level to compare the R/L classifier with the [R/L]+[G/B-p] and [R/L]+[G/B-erp] classifiers as well. Our results show that R/L when combined with the G/B (either power, erp or power and erp) classifier outperforms the R/L classifier significantly for all participants except for participant 3. It is worth noting that participant 3 has G/B-p and G/B-erp classification rates very close to chance level (refer to Table 3) and it is not surprising that the combined classifiers do not outperform the R/L classifier. Interestingly, though, the performance of the combined classifier for this participant is not worse than our baseline R/L classifier. For easier visual comparison, the results of R/L in the second column and [R/L]+[G/Bp]+[G/B-erp] in the last column are plotted as a bar plot for each participant in Figure 3.5. Our results show an average of 11% improvement in classification accuracy across 10 participants.

Table 3.4: Classification results for combined classifier across frequency bands. The first number is the mean classification rate over three instances of 10-fold nested cross validation and the second number is the standard error. Whenever the results in the right-most column are significantly higher than the R/L results, numbers are specified in bold.

Participant	R/L	R/L+G/B-p	R/L+G/B-erp	R/L+G/B-p+G/B-erp
One	0.87 / 0.005	0.89 / 0.006	0.90 / 0.005	**0.91 / 0.006**
Two	0.60 / 0.010	0.76 / 0.009	0.75 / 0.011	**0.78 / 0.006**
Three	0.68 / 0.012	0.68 / 0.008	0.67 / 0.010	0.68 / 0.010
Four	0.68 / 0.010	0.79 / 0.008	0.80 / 0.009	**0.84 / 0.008**
Five	0.73 / 0.010	0.76 / 0.009	0.78 / 0.008	**0.80 / 0.007**
Six	0.63 / 0.012	0.71 / 0.011	0.73 / 0.007	**0.75 / 0.009**
Seven	0.78 / 0.009	0.84 / 0.008	0.83 / 0.007	**0.87 / 0.007**
Eight	0.79 / 0.010	0.81 / 0.007	0.83 / 0.008	**0.84 / 0.009**
Nine	0.60 / 0.011	0.77 / 0.009	0.75 / 0.009	**0.82 / 0.008**
Ten	0.57 / 0.010	0.69 / 0.009	0.70 / 0.009	**0.74 / 0.009**

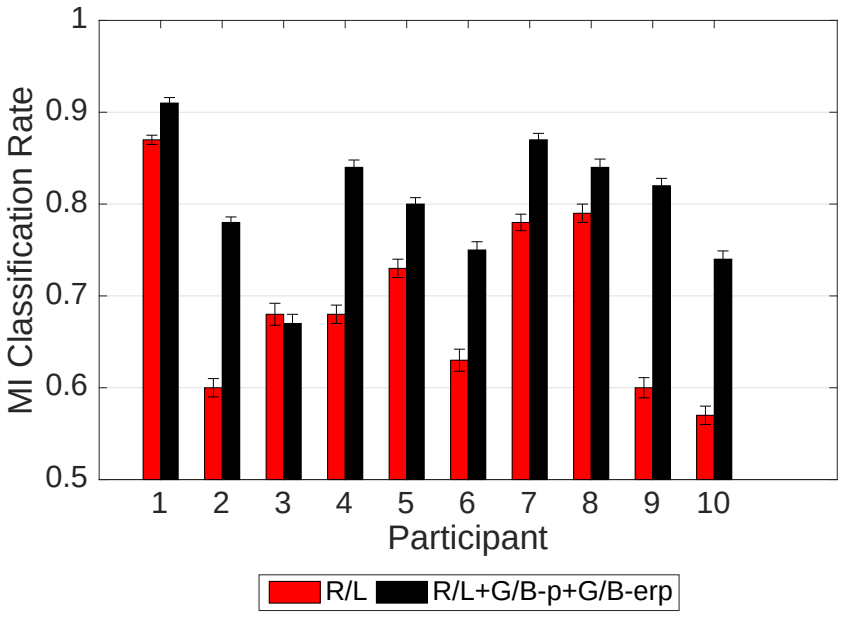

Figure 3.5: Comparison of across-the-frequency-bands [R/L] and [R/L]+[G/B-p]+[G/B-erp] classifies, from Table 3.4.

3.5 Discussion and conclusion

In this study we investigated error-related spectral perturbation to parse out the effect of error-related brain processes that may occur in the same frequency bands as the motor imagery signal. There are many studies in the literature that show the effect of feedback in EEG-based BCI performance [49, 50, 51, 52, 53, 10, 54, 55, 57, 17, 18, 69, 60]; however, we believe that the use of learned error-related signals from multiple spectral bands and spatial locations combined with active BCI signals through learned weighted voting is unique. The learned weighted voting (for combining R/L and G/B) lets both the error-related features and the active BCI features (motor imagery in our case) have influence at the same time with the flexibility to let the classifier adjust to each participant individually. It is worth emphasizing that, at least in our 10 participants, combining R/L with G/B-p and G/B-erp is not harmful even for participants with relatively poor G/B classification.

In this study, we used a sham feedback paradigm where the participants were presented pre-determined cursor movements but were misled to believe that they were in control. Note that we do not propose that sham feedback should be used during the operation of real BCIs. The sham feedback was important here to have adequate number of good and bad cursor movements to train the G/B classifier for all participants independent of the participant's motor imagery performance. We hypothesize that during real online MI use, the users response to cursor movements will similarly be discriminative to feedback polarity and that a combined classification system, as proposed in this work, will give improved performance for predicting desired target locations.

Although in this work we have considered a right/left-hand motor imagery paradigm, we believe that our approach is generalizable to other classes of motor imagery, other BCI modalities and perhaps other BCI paradigms. For instance, it would be interesting to look for similar G/B classifiability in other BCI modalities such as those based on functional near-infrared spec-

troscopy signals [70, 71]. In a recent study by Stivers et al. [72], low-frequency time-domain error-related features were used in a G/B classifier in a speller. In another study [73], Zeyl et al. demonstrated the application of error-related potentials below 20 Hz in an auditory BCI. In both these examples as well as in other BCI paradigms such as P300 or SSVEP BCIs [46, 47], it would be interesting to look for G/B signals in higher-frequency bands.

Traditional active cursor-control BCI systems use explicit control strategies, i.e. they use only R/L-type classifiers to detect motor imagery mapped to cursor movements. Zander et al. [74] in a recent study demonstrated neuroadaptive technology for implicit cursor control. Using passive BCI [62, 63], the participants controlled a cursor through passively changing future cursor movements based on an error-related potential-type signal, without any type of explicit communication or control. In our current work, we demonstrated an active R/L control combined with passive G/B classifier using a wider range of features from low to high frequency bands. As one final variation, de Sa [75, 76] proposed that active motor imagery can also be mapped to G/B-type commands (e.g. left-hand MI meaning change direction and right-hand MI meaning stay on course), and theoretically demonstrated increased robustness compared to direct control. For future work, we are interested in how these four strategies compare to each other in a uniform cursor-control paradigm, in terms of performance and other metrics such as user satisfaction and ease of use.

We are interested in investigating the generalizability of the G/B classifier across changes in task condition. For instance, do participants produce similar patterns of G/B across multiple sessions or when task workload varies? Omedes et al. showed this in lower-frequency bands across various tasks [58] and associated it with error-related potentials, but they have not discussed this for higher-frequency bands. A related interesting question would be to investigate the underlying brain networks that are involved in generating the good/bad signal(s).

3.6 Acknowledgments

This work was supported by the NSF grants IIS 1219200, SMA 1041755, IIS 1528214, UCSD FISP G2171, and NIH grant R01NR013500.

Chapter Acknowledgments

Chapter 3, in full, is a reprint of material as it appears in Mahta Mousavi, Adam S. Koerner, Qiong Zhang, Eunho Noh, and Virginia R. de Sa. "Improving motor imagery BCI with user response to feedback," Brain-Computer Interfaces 4, no. 1-2 (2017): 74-86. The dissertation author was the primary author of this publication. The copyright for this publication is owned by Brain-Computer Interfaces Journal (Taylor and Francis Group) and used in accordance with their terms and conditions.

Chapter 4

Improving real-time BCI control using the error-related brain activity

4.1 Abstract

Brain-computer interface systems read and interpret brain activity directly from the brain. They can provide a means of communication for patients suffering from locked-in syndrome as perhaps the only available solution. However, these systems are currently limited to laboratory environments. One major challenge in translating existing systems to the everyday lives of patients is the non-stationarity of brain activity. This limits the reliable transfer of algorithms that are trained during a calibration session to real-time BCI control. One source of non-stationarity is the user brain response to BCI output (feedback), i.e. whether the BCI feedback is perceived as an error by the user or not. In this work, we demonstrate a real-time implementation of our earlier proposed motor imagery BCI combining the information from the motor imagery signal and the error-related brain activity in a novel way so as to gain benefit from both sources. Our results show significantly improved BCI performance in real-time BCI control across 12 participants, compared to a conventional motor imagery BCI.

4.2 Introduction

Since the introduction of the concept of a brain-computer interface (BCI) by Vidal [1], there have been many implementations of it as potential communication or rehabilitative interventions for patients (e.g. [2, 3, 4, 5]). Motor imagery (MI) BCI is one category of BCI systems that relies on the user-initiated movement imagination of different body parts that result in distinguishable brain patterns [3, 8].

Nevertheless, so far, very few examples have left the laboratory environment to be used by patients in need to improve the quality of their daily activities [77, 78]. In the case of non-invasive BCIs using electroencephalography (EEG), lack of robustness and reliability are major limitations [7]. This lack of reliability partly owes itself to the non-stationarity of brain activity that limits the transfer of a classifier trained during calibration to a real-time control session [79].

To improve reliability in BCI control, one approach is to use other available sources of information in order to support, adjust, or correct the information coming from the MI signal. One potential such source is the brain activity in response to the BCI output (feedback). It is shown in the literature that user brain activity is in fact different when observing a successful execution of an intended task by the BCI versus an unsuccessful execution [10, 11, 12, 36]. This information is classifiable and can be used to alleviate the reliability limitation [80, 51, 36].

There are multiple approaches as how to use the feedback-related brain activity to improve BCI performance. One approach is to discard a BCI output and repeat the trial upon detection of an error [11, 13]. A second approach, based on error-driven learning, attempts at limiting the occurrence of a future error by updating the classifiers upon the detection of error-related brain activity or to discard the unsupervised adaptation using the recent data if an error is detected [15, 16]. A third approach, based on error integration [17, 18], proposed a motor imagery BCI for 1-D cursor control that integrates the user brain activity in response to the changes in the observed direction of cursor movement.

Recent studies in invasive BCIs also show evidence for the possible detection of error-related brain activity and propose to use it to improve BCI performance. For instance, in [81], the authors showed that error signals can be detected from human electrocorticography (ECoG) in a continuous task comprising a video game. In another work [82], the authors showed the detection of error-related brain activity in a motor imagery task in human ECoG. Moreover, in [83], the authors proposed to augment an intracortical BCI with error detection. They showed in an experiment with primates that a classifiable error signal can be detected from electrodes located in the premotor and primary motor cortices and proposed a system to automatically undo or prevent mistakes.

In an earlier work, in a motor imagery BCI system, we introduced a more sophisticated error integration approach [17, 18] by considering the error-related brain activity as a separate cognitive process and combined a right/left hand motor imagery classifier with a classifier detecting whether the user perceived the last BCI output as error or not [36]. The proposed hybrid BCI system translated the classification score from the domain of the error-related brain activity to the motor imagery score domain and learned a logistic regression to best combine the two sources of information for each user. This allows for a system that relies more/less on either of the motor imagery or error-related brain activity signals depending on how reliable each source of information is for a specific user. In our earlier work, we showed the efficacy of such a system in a BCI with sham feedback across 10 participants [36].

In this work, we demonstrate the efficacy of our proposed approach in a real-time motor imagery BCI. Across 12 participants, we show significantly improved performance compared to a conventional motor imagery BCI that does not use the error-related brain activity. Further analysis of the results show that in fact the error-related brain activity classifier is more consistent throughout the session as opposed to the motor imagery classifier. This demonstrates that the error-related brain activity is a more reliable source of information that can be used to improve the overall BCI performance.

4.3 Methods

The study was approved by the University Institutional Review Board at UC San Diego and all participants signed an informed consent form prior to their participation. Data were recorded from 12 naive participants participating in a motor imagery BCI study. Each participant participated in one session of roughly 2.5 hours in length. Participants comfortably sat in front of a screen, centered with respect to the screen and about one meter away from it. Each session comprised of two phases described in detail next.

4.3.1 Paradigm

The first phase was primarily designed for the participants to gain experience with the motor imagery of their right/left hand. Each trial began by showing a right/left arrow representing the side of imagery. Next, participants imagined movement of the corresponding hand for 3 seconds while visually focusing on a plus sign in the center of the screen to minimize eye movement artifacts. At the end of each trial, participants were provided with feedback in the form of two bars whose height represented the power in 7–30 Hz frequency band averaged on their right (EEG channels FC4, C4, CP4) and left (EEG channels FC3, C3, CP3) motor cortices, separately. Participants were instructed to maximize the bar on the side of imagery and minimize the one on the other side [84]. There was a 5-second break before the next trial began. There were a total of 30 trials in this phase (15 right and 15 left motor imagery) divided into three blocks. Participants were given instructions and suggestions on what to imagine for their hand movements; however, they had a chance to explore different movements and decide on what works best for them during this phase. After each block, participants could take as much rest as needed.

After this phase, participants filled in a short questionnaire in which they answered what movement they imagined for their right and left hands. They were instructed not to change their selected movement imagination throughout the rest of the experiment.

In phase 2, participants were instructed to use their selected right/left movement imagination to move a cursor to the right/left towards a target. An example of a trial is presented in Figure 3.1. This phase was comprised of 9 blocks and each block comprised of 20 trials. The target appeared randomly at the right or the left side while maintaining that each block comprised of 10 right and 10 left trials.

In the first three blocks, participants received sham feedback while they were led to believe that they were in control of the cursor movements. However, the cursor movements were predefined and randomly generated with the following criteria: the cursor had a fixed probability of going towards the target (p=0.6) following a Bernoulli distribution; if the generated sequence for a trial had more than three consecutive changes in direction or was longer than 12 movements without hitting the target or the other end, the sequence was regenerated. The movement sequence for the first three blocks was generated ahead of time and was kept the same across participants. The recorded EEG data in the first three blocks were used for calibration of the classifiers – as explained in detail in the next subsection.

In the latter 6 blocks, participants received real online feedback in which 3 blocks used right/left hand motor imagery (R/L) control and the remaining 3 blocks used our proposed BCI control that combined the right/left hand motor imagery with the error-related brain activity signal (called a good/bad classifier as it detects whether the user perceived the last cursor movement as good, i.e. going towards the target, or bad, i.e. going away from the target). The proposed control is therefore called R/L+G/B control. R/L and R/L+G/B blocks were alternating and the order was counterbalanced across participants. The maximum number of allowed movements in each trial was set to 12. If the cursor hit the target or the other end or if the cursor had reached its maximum number of allowed jumps, the trial would be over and the next one would start. There was a 5-second break after each trial before the next trial began.

Participants were not aware of the sham feedback in the first three blocks and the different controls in the online blocks. After each block in phase 2 (including the calibration and online

control blocks), participants answered the following question: *from 1 to 10 where 1 represents the least and 10 the most amount of control, how much in control of the cursor did you feel?*

Participants also filled in questionnaires aimed at quantifying their handedness and various aspects of their personality [85, 86, 87, 88]. However, the data were not used for the analysis that is presented next.

4.3.2 Classifiers

Calibration

At the end of the first three (calibration) blocks, R/L and R/L+G/B classifiers were trained. To do so, first the trials were downsampled to 100 Hz, epoched 0–1 seconds after each cursor movement and filtered with an IIR filter (6th order butterworth) in different frequency bands that are explained next. We used the filtfilt function from SciPy [89] that applies a filter twice, once forward and once backwards, to ensure zero-phase filtering.

Three classifiers were trained. For the right/left hand motor imagery classification (R/L), the epoched data were filtered to 7–30 Hz. Then the method of common spatial patterns (CSP) [19] was used and the top 3 CSP filters for the right and left classes were selected. Filtered epochs were passed through the selected CSP filters and the logarithm of the variance of the filtered data across time were selected as features. A linear discriminant analysis (LDA) was trained on the selected features.

For the G/B classifier, we used two different methods. We filtered the data to 1–30 Hz frequency band, epoched 50–950 ms and used the same CSP technique as explained earlier, to capture the spatial features of the good/bad signal. This is called the G/B-csp classifier. Note that this classifier is very similar to the G/B-p classifier described in Chapter 3 but uses a single frequency band. This is to have fewer number of trainable parameters to allow for a shorter calibration phase.

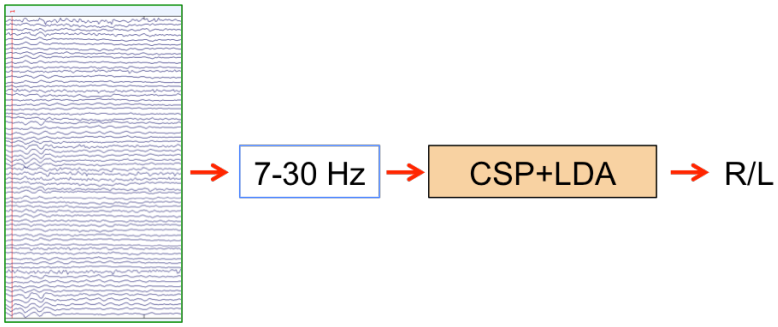

Figure 4.1: R/L control.

We trained another G/B classifier called G/B-wm following the windowed-means approach for event-related potential (ERP) single trial classification to capture temporal features [90, 11]. We considered EEG activity on channels Fz, Cz, CPz and Pz as the error-related brain activity is known to be a fronto-central signal that is best picked up by the mid-line channels [11]. EEG signal on these 4 channels were filtered to 1–10 Hz and baselined to the first 50 ms. Then the average of the signal in 100 ms non-overlapping windows in 9 windows (50–950 ms) were selected as features. An LDA was trained on the selected features. Note that G/B-wm is very similar to the G/B-erp classifier described in Chapter 3 but uses fewer number of windows .

Our proposed BCI combines the scores from R/L and G/B classifiers (G/B-csp and G/B-wm). During calibration, a logistic regression was trained on the scores from the R/L, G/B-csp and G/B-wm classifiers using the cursor direction of movement as explained in section 3.3.3.

Online control

As mentioned earlier, blocks 4-9 comprise of online control of the cursor where half of them use R/L control and the rest use R/L+G/B control.

In the R/L control blocks, the R/L classifier is used to control the cursor the same way as in a conventional motor imagery BCI. This is depicted in Figure 4.1.

In the R/L+G/B blocks, the scores from the R/L, G/B-csp and G/B-wm classifiers were combined based on the cursor direction of movement (CD) and through a logistic regression.

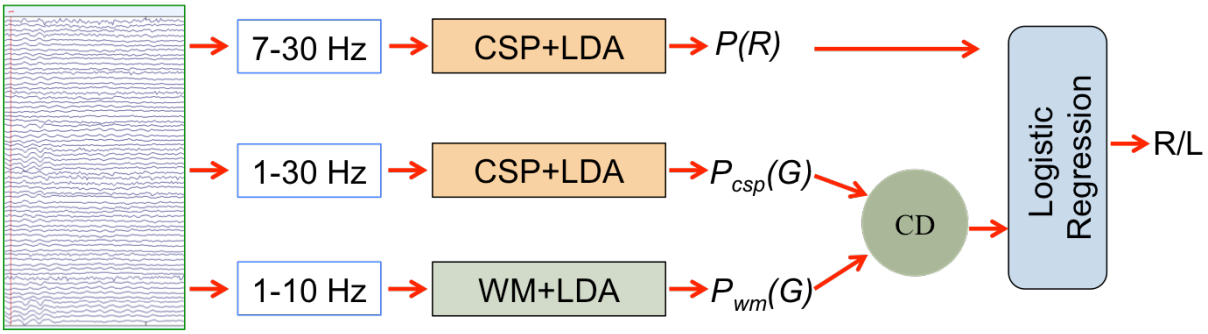

Figure 4.2: R/L+G/B control. CD indicates the cursor direction of movement. $P(R)$ indicates the score of the R/L classifier, i.e. probability of right. $P_{csp}(G)$ and $P_{wm}(G)$ indicate the scores of the G/B-csp amd G/B-wm classifiers, respectively. If the cursor moves to the right, $P(R)$, $P_{csp}(G)$ and $P_{wm}(G)$ will be combined through the logistic regression. However, if the cursor moves to the left, $P(R)$, $1-P_{csp}(G)$ and $1-P_{wm}(G)$ will be combined. This is explained further in section 3.3.3.

This is depicted in Figure 4.2.

4.3.3 Data collection and processing

EEG data were recorded using a 64-channel BrainAmp system (Brain Products GmbH). The active electrodes were located according to the international 10–20 system [65]. Electromyography (EMG) data were also recorded with bipolar electrodes using BrainAmp ExG from the wrists and upper forearms as depicted in Figure 3.1. Data were recorded at a sampling rate of 5000 Hz. To ensure accurate recording and inference of the brain activity, a small photo sensor was placed at the bottom right corner of the screen and was connected to the ExG box. A white circle (with the same diameter as the the photo sensor) was turned on and off at the same time that the cursor moved on the screen. This allowed us to record an accurate stimuli presentation time and remove any potential jitter in the measurement system.

Codes were written in Python. Simulation and Neuroscience Application Platform (SNAP) [34] was used for stimuli presentation, Lab Streaming Layer (LSL) [91] to interface the EEG system with the computer, and Numpy [92], SciPy [89] and scikit-learn [93] for the rest of the calibration and online data processing.

All trials from the calibration phase were used to train the classifiers. For the offline analysis of the recorded data from the online control phase, in participants B5 and B6, data from 3 and 2 trials were removed respectively due to technical issues during recording. MATLAB [94] and EEGLAB [38] were used for offline epoching and plotting of the results. Python was used for the offline analysis.

4.3.4 Metrics

We compared R/L and R/L+G/B controls in various aspects. As mentioned earlier, trials began with the cursor at the center of the screen and the target at either end. A successful trial is when the cursor hits the target. 'Hit rate (HR)' is defined as the success rate in each block (of 20 trials). We define another online score comprised of the participants' ratings of how much in control they felt in each block. We call this 'subjective rate (SR)'. We report the participants' online scores including hit rates and their subjective rates.

Moreover, classification accuracy for each cursor movement is reported from offline analysis of the recorded data. We call every cursor movement a 'step'. A single trial is comprised of multiple steps. Since in the calibration phase, the classifiers were trained on every step, it is necessary to compare the online classification accuracy for each step as well.

4.4 Results and discussion

4.4.1 Online scores

Figure 4.3 reports the online hit rates (HR) and subjective rates (SR) across participants. For each participant, the online part of our experiment comprised of 6 blocks (3 R/L and 3 R/L+G/B blocks). Scores were averaged across the R/L and R/L+G/B separately and reported as HR and SR for the corresponding controls. Error bars show the standard error of the mean.

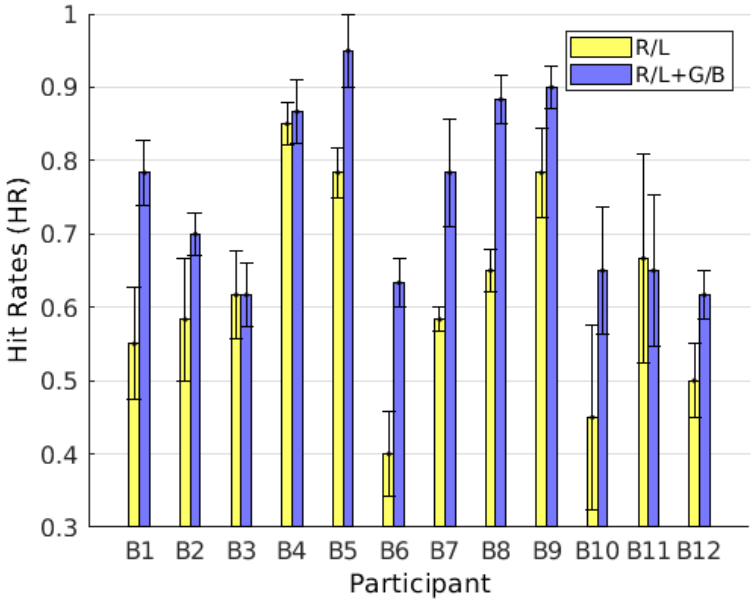

(a) Online hit rates (HR).

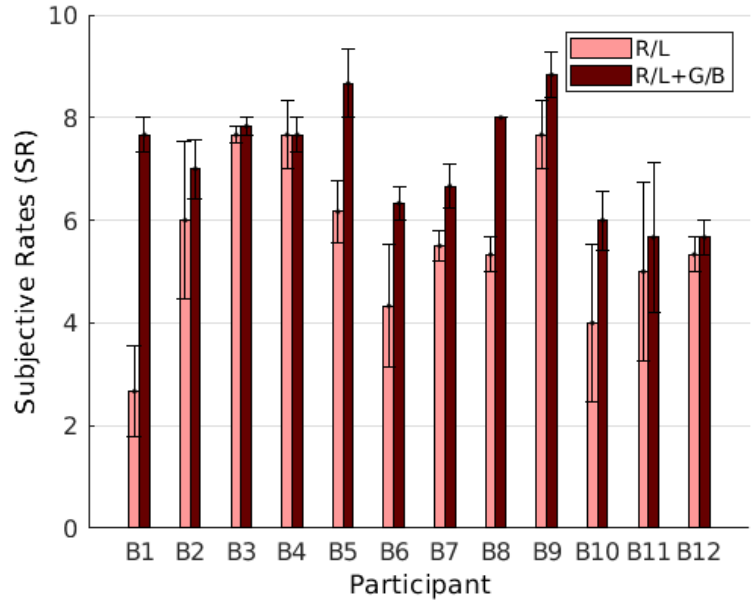

(b) Subjective rates (SR).

Figure 4.3: The bar heights represent the average online scores of R/L and R/L+G/B blocks across participants. Error bars show the standard error of the mean. Paired-sampled t-tests indicate that R/L+G/B performs significantly better than R/L in both online hit rates and subjective rates (paired-sample t-test, $p < 0.001$ and $p = 0.003$ respectively).

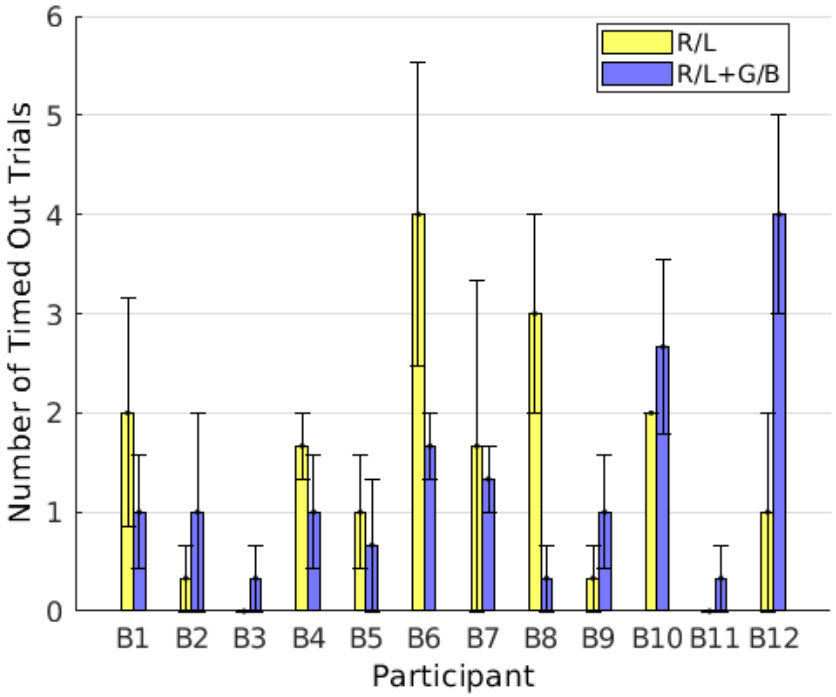

Figure 4.4: The bar heights represent the average number of timed-out trials per block in R/L and R/L+G/B blocks for each participant. Error bars show the standard error of the mean. Paired-sample t-test shows no significant difference across participants in the number of timed-out trials (p=0.75) in R/L and R/L+G/B blocks. Note that every block has 20 trials.

Paired-sample t-tests indicate that the HR and SR are both significantly better in R/L+G/B blocks than in R/L blocks indicating a more reliable control in the proposed BCI both objectively and subjectively (paired-sample t-test, $p < 0.005$).

As mentioned earlier, trials could end when the number of cursor movements reaches its maximum (i.e. 12 movements). Figure 4.4 shows the average number of timed-out trials for R/L and R/L+G/B blocks. A paired-sample t-test shows no significant difference across participants in the number of timed-out trials (p=0.75) in R/L and R/L+G/B blocks.

4.4.2 Transfer of R/L and G/B classifiers from calibration to online data

After the experiment, we performed additional offline analyses to compare the performance of the classifiers. The classification accuracy in every step resulting from the R/L, G/B-

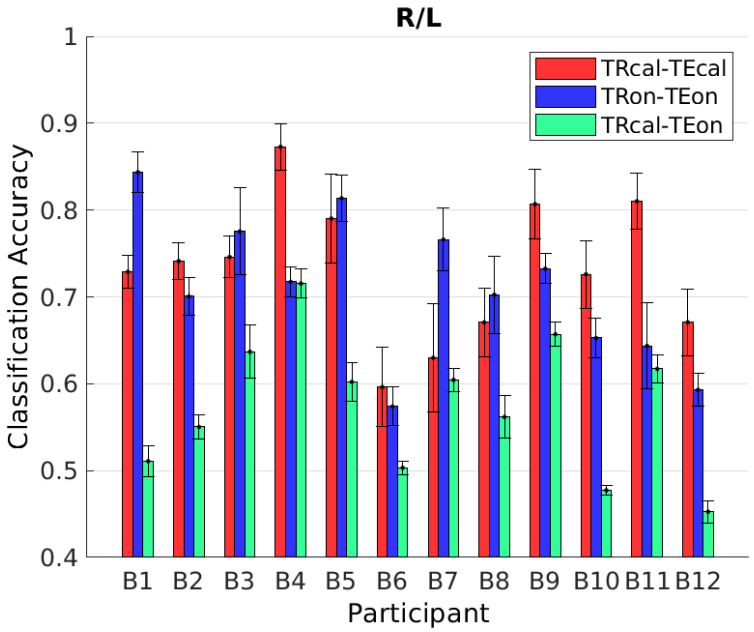

Figure 4.5: The transferability of the R/L classifier from calibration data to online data. The red and blue bars in each plot indicate the cross-validation accuracy on calibration and online data respectively. The red bars are significantly better than the green bars for the R/L classifier across participants (paired-sample t-test, $p<0.001$).

csp and G/B-wm is reported in Figures 4.5 and 4.6. The red bars represent the accuracy of a classifier trained and tested on calibration data. The blue bars on the other hand, represent the accuracy of a classifier trained and tested on the online data steps. Both blue and red bar heights indicate the average of a 5-fold cross-validation accuracy over balanced classes. Classes were balanced by subsampling the larger class and this was done 10 times. Therefore, bars represent the average and the error bars indicate the standard deviation.

The green bars represent the classification accuracy of a classifier trained on the calibration steps and tested on the online steps, again over balanced classes. Classes were balanced by subsampling the larger class and this was done 10 times. Therefore, bar heights represent the average and the error bars indicate the standard deviation. Note that we did not separate R/L and R/L+G/B blocks' steps in this analysis.

Even though the red bars on average are lower in both G/B-csp and G/B-wm compared

to the red bars in the R/L plot, the loss from transferring the classifier to online data is much larger for the R/L classifier. We used paired-sample t-tests to compare the classification accuracy across participants comparing the red bars and green bars for each classifier. For G/B-csp and G/B-wm, the difference is not statistically significant across participants (paired-sample t-test, $p>0.2$). However, for R/L classifier, the green bars are significantly worse than the red bars and this difference is statistically significant across participants (paired-sample t-test, $p<0.001$).

We also compared the red bars and the blue bars (a classifier trained and tested on calibration data versus a classifier that is trained and tested on the online data). The reason is because one can argue that the lower performance as represented by the green bars (i.e., the performance of a classifier that is trained on calibration data and tested on online data) is mainly because the data quality is different and less classifiable in the online data. We argue that this is not the case. In fact, the difference between the red bars and blue bars for the R/L classifier across participants is not statistically significant (paired-sample t-test, $p>0.3$) suggesting that the R/L data quality is not the cause of the drop in the green bars.

4.5 Conclusions

In this work, we demonstrated a novel approach to utilize error-related brain activity in a real-time motor imagery BCI to improve the overall BCI performance. We showed that across 12 participants, they were able to control the BCI using the proposed method significantly better than the conventional motor imagery BCI. We showed this improvement is significant in terms of the average hit rates as well as subjective ratings.

Furthermore, we showed that the error-related brain activity classifiers (G/B-csp and G/B-wm) are both better transferred from calibration to the online control. At the same time, the performance of the motor imagery classifier (R/L) drops when transferred from calibration to the online control. In other words, the error-related brain activity classifiers are more reliable

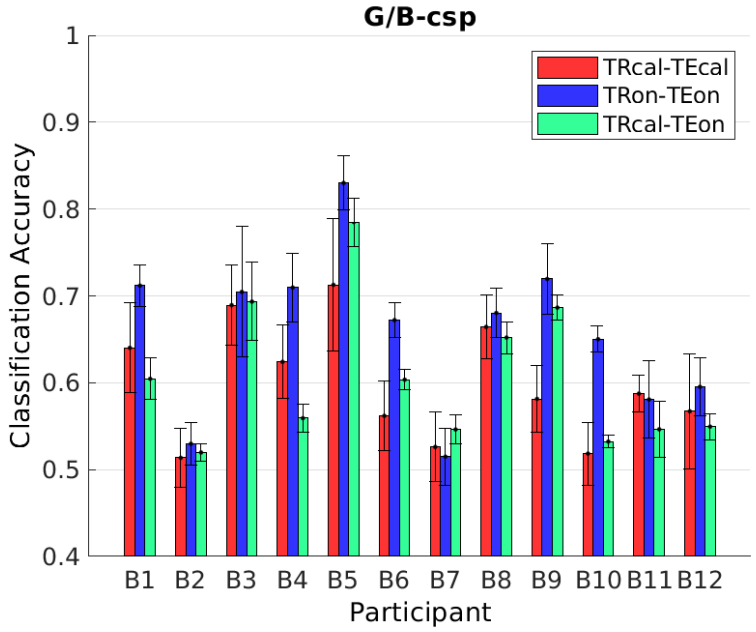

(a)

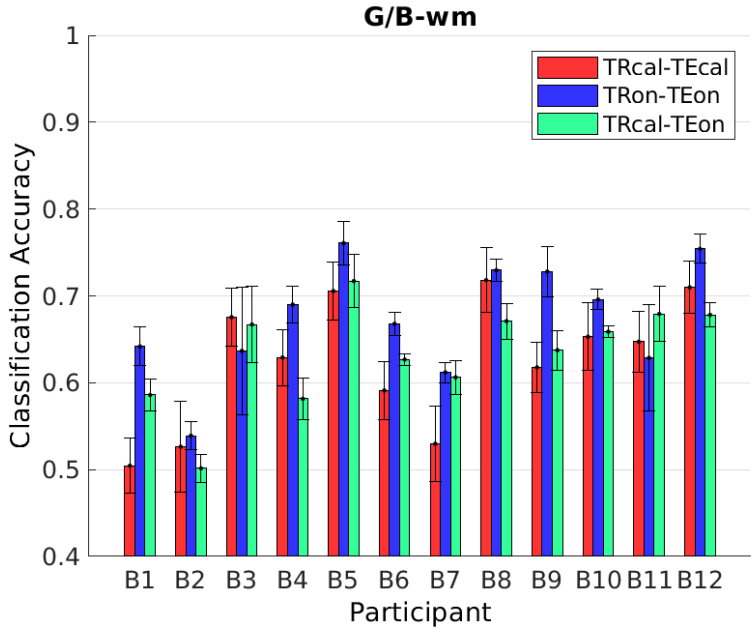

(b)

Figure 4.6: The transferability of the G/B-CSP and G/B-WM classifiers from calibration data to online data. The red and blue bars in each plot indicate the cross-validation accuracy on calibration and online data respectively. The blue and green bars are not significantly different across participants for G/B-CSP and G/B-WM classifiers (paired-sample t-test, $p>0.2$).

(consistent over time from calibration to online use) than the motor imagery classifier. We believe that this is in part due to the drift in the EEG data, but also in part due to the fact that some participants performed worse than the sham calibration feedback and were possibly discouraged at times during the online control – as mentioned earlier, during calibration, participants were provided with sham feedback but were not aware of it.

Other works in the literature also point out that the error-related brain activity results in a reliable classifier over time [54, 95] allowing for a more reliable source of information for an improved BCI performance as we showed in this work. Future work can shed light on why the performance of the classifier based on the motor imagery signal is not consistent as opposed to the error-related brain activity classifier. This can allow us to better understand the interaction between the two sources of information and hopefully direct us to design an even more reliable BCI system.

Chapter Acknowledgments

Chapter 4, in part, will be submitted for publication as Mahta Mousavi, Laurens R. Krol, and Virginia R. de Sa. "A novel hybrid motor imagery BCI using error-related brain activity." (This is the working title and it may change upon submission). The dissertation author is the primary investigator and author of this work.

Chapter 5

Spatio-temporal analysis of the motor imagery signal

5.1 Abstract

Brain-computer interface (BCI) systems are proposed as a means of communication for locked-in patients. One common BCI paradigm is motor imagery in which the user controls a BCI by imagining movements of different body parts. It is known that imagining different body parts results in event-related desynchronization (ERD) in various frequency bands. Existing methods such as common spatial patterns (CSP) and its refinement filter bank common spatial patterns (FB-CSP) aim at finding features that are informative for classification of the motor imagery class. Our proposed method is a temporally adaptive common spatial patterns implementation of the commonly used filter-bank common spatial patterns method using convolutional neural networks; hence it is called TA-CSPNN. With this method we aim to: (1) make the feature extraction and classification end-to-end, (2) base it on the way CSP/FBCSP extracts relevant features, and finally, (3) reduce the number of trainable parameters compared to existing deep learning methods to improve generalizability in noisy data such as EEG. More importantly,

we show that this reduction in parameters does not affect performance and in fact the trained network generalizes better for data from some participants. We show our results on two datasets, one publicly available from BCI Competition IV, dataset 2a and another in-house motor imagery dataset.

5.2 Introduction

Brain-computer interface (BCI) systems read and interpret brain signals directly from the brain and were proposed originally as communication methods for patients suffering from locked-in syndrome [2]. Motor-imagery (MI) based BCIs involve the user imagining moving different body parts to provide different control signals. This results in decreased/increased power in some frequency bands often referred to as event-related desynchronization/synchronization (ERD/S) [24, 3], and the differences between MI of different body parts can be emphasized with spatial filtering. The common spatial patterns (CSP) algorithm is commonly used to find filters that maximize the projected variance for one class while minimizing it for the other class [96]. Filter-bank common spatial patterns (FB-CSP) is a variation of CSP in which optimal sets of filters are sought in multiple frequency bands [20]. However, one downside of both CSP and FB-CSP methods is that supervised feature extraction step (finding the optimal filters) and classification are performed in separate steps.

Convolutional neural networks (CNN) have revolutionized the area of computer vision [97]. However, the characteristics of EEG signals are very different from those of images, videos, or speech. EEG signals are time series recorded from electrodes located at multiple sites on the scalp. They are prone to artifacts from non-brain sources such as eye and muscle movements and usually have low signal-to-noise ratio. Therefore, the common architectures of deep convolutional neural networks should be adapted to provide their benefits (end-to-end feature extraction and classification and ability to learn non-linear task specific classification boundaries) while not

suffering from the potential drawbacks (overfitting or learning to use class-correlated non-brain artifacts for classification).

Proposed by Maryanovsky et. al [21], CSP-NN implements the CSP algorithm in a convolutional layer (with kernel size C $\times$ 1) followed by squared-average pooling to emulate the usual squared post-processing after CSP filtering. It independently computes spatial filters for multiple frequency bands using signals that are already filtered through a bank of band-pass filters just as the original filter-bank CSP algorithm does. Then the features from the filters are merged and go through a fully-connected layer before the output layer.

Shallow and deep ConvNets [98] are two CNN-based architectures proposed for EEG-based BCI data classification. Shallow ConvNet learns a temporal convolution as its first layer and a spatial convolution afterwards. A squared-average pooling layer provides non-linearity; however, the pool that is averaged and squared is shorter than the length of the EEG epoch. Next, the features are concatenated and their logarithm is sent to a dense layer with soft max activation over the number of units equal to the number of motor imagery classes.

EEGNet [99] was proposed as a general-purpose CNN-based model for EEG-based BCIs and can handle both ERD/ERS type features as well as temporal event-related potentials (ERP). It consists of two blocks, each with convolutional layers, non-linear activation function (exponential linear unit), pooling and dropout. The EEGNet architecture has fewer parameters than shallow ConvNet.

As motor imagery BCIs are known to involve changes in power in different frequency bands, we propose an architecture for ERD/ERS type features. It is important to note that since EEG is generally noisy and artificial neural networks can use many parameters to learn highly non-linear functions, they are prone to overfitting. Inspired by the FB-CSP method, our goal is to propose a CNN-based model for motor imagery classification that keeps the number of parameters small without compromising performance. We propose to use the temporal convolutional layer from EEGNet together with the spatial feature extraction convolutional layer and activation

function from CSP-NN. We call this temporally adaptive common spatial patterns with neural networks (TA-CSPNN). This method uses about half the parameters of EEGNet and yet provides similar or improved results (see Section 5.5).

5.3 Proposed architecture: TA-CSPNN

Let $X_i \in R^{C\times T}$ be the available EEG epochs for each class $i \in \{1,...,N\}$ where N is the number of imagery classes, C is the number of EEG channels and T the number of time samples. Layers in TA-CSPNN are described in Table 5.1 and in a block diagram in Figure 5.1. The design parameters are K: length of temporal kernel, F_t: number of temporal filters, F_s: number of spatial filters, and p: dropout layer parameter that indicates the fraction of layer inputs to drop [100].

Table 5.1: Description of layers in TA-CSPNN.

Layer	Filters/Units	Size	Output
Input	-	-	$(1,C,T)$
Conv 2D	F_t	$(1,K)$	(F_t,C,T)
Batch Normalization	-	-	(F_t,C,T)
Depthwise Conv 2D	F_s	$(C,1)$	$(F_t\times F_s,1,T)$
Batch Normalization	-	-	$(F_t\times F_s,1,T)$
Activation: x^2	-	-	$(F_t\times F_s,1,T)$
Average pooling	-	-	$(F_t\times F_s,1,1)$
Dropout(p)	-	-	$(F_t\times F_s,1,1)$
Flatten	-	-	$F_t\times F_s$
Fully connected	N	-	N
Activation: Softmax	-	-	N

The first convolutional layer filters the input EEG signal with multiple filters. Note that this layer is equivalent to filtering each channel of EEG data with a finite impulse response (FIR) filter:

$$X_i(c,t) = \sum_{n=0}^{K-1} b_n X_i(c,t-n), \tag{5.1}$$

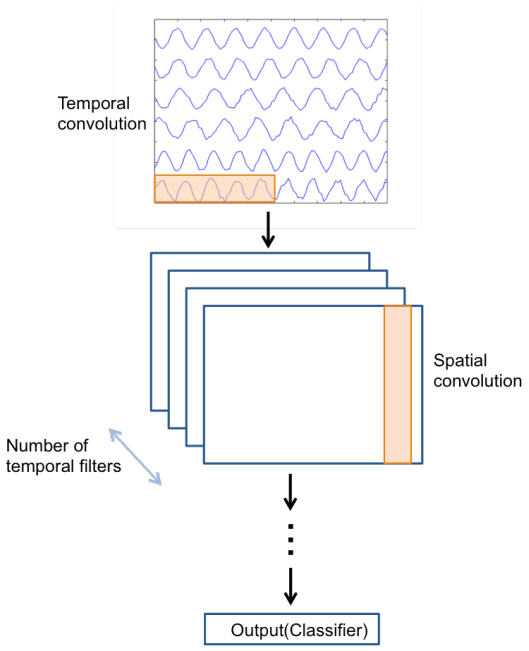

Figure 5.1: Block diagram of the proposed TA-CSPNN.

where K is the length of the temporal filter and b_n $(n \in \{0, ..., K-1\})$ the filter weights. We did not use a bias for the weights trained in this layer to be as close to equation 5.1 as possible. Note that this temporal Conv2D is implemented with mode 'same' in Keras to pad the input with zeros such that the output has the same number of rows and columns as the input. Batch normalization [101] along the first dimension is applied next. Then a depthwise 2D convolution is applied to extract spatial features. This is equivalent to learning the spatial filters in each temporally filtered (filter bank) separately. We used a norm constraint on the spatial filter weights such that $||w||_2 \leq 1$. This is because the common spatial filters in the CSP algorithm are eigenvectors of a generalized eigenvalue problem and have norm 1. Note that this Conv2D layer is only applied along the channels (and not the time dimension) and is essentially a one-dimensional kernel. Common spatio-temporal filters can be learned by using a 2D kernel along time and space as discussed in [21].

The output of the spatial convolution is squared and summed (average pooling layer) across time which is equivalent to calculating the power of the spatially filtered EEG data. The

dropout layer [100] comes after. We use dropout to prevent overfitting and allow better generalization. Finally the features are sent through a dense layer of the size of the number of imagery classes (output). The activation is chosen to be softmax such that the network outputs probabilities.

As mentioned earlier, activity from the spatial convolution layer is squared and passed through an average pooling layer. This is different from EEGNet's use of the exponential linear unit (ELU) activation function. Figure 5.2 plots both of these functions. We chose x^2 as the non-linear activation function since ERS/ERD features are variations in the power of the EEG signal.

Code was implemented in Keras [102] with Tensorflow backend [103] and is available at `https://github.com/mahtamsv/TA-CSPNN` .

We used Adam optimization with default parameters [104] to minimize the categorical cross-entropy loss function. In all experiments, 10% of the training data were used for validation. To avoid overfitting, the accuracy of the validation set was monitored for early stopping [105] with a patience of 50 and maximum of 500 epochs. The model was then evaluated on the test set.

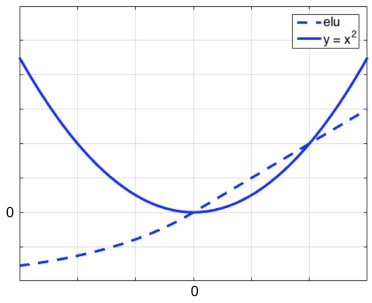

Figure 5.2: Comparison of ELU and x^2 activations.

5.4 Datasets

We report the performance of our proposed architecture on two datasets:

5.4.1 Dataset I

This is a publicly available dataset (BCI Competition IV, Dataset 2a) [106] from 9 participants performing left hand, right hand, both feet, and tongue motor imagery. The dataset consists of data from two sessions (train and evaluation sets) for each participant recorded on two different days. Each session has 288 trials total (72 for each imagery class). Data were recorded from 22 EEG and 2 EOG channels but we only used the EEG channels.

We used code provided by [98] to import, epoch and filter the data from 4–40 Hz and epoch from 0.5–2.5 seconds after the onset of the cue. The number of classes is $N = 4$. Data on each channel were downsampled to 125 Hz.

5.4.2 Dataset II

Motor imagery data were recorded from 10 participants who signed a consent form approved by the UC San Diego Human Research Protections Program prior to participating in the experiment. Data were recorded using a 64-channel BrainAmp system (Brain Products GmbH). Participants were instructed to perform right/left hand motor imagery to move a cursor on the screen in front of them right/left towards a target at either the right/left side of the screen. The cursor moved at the speed of one step per second towards/away from the target. After visual inspection, we applied ICA and removed eye and muscle artifacts. Then the data were downsampled to 100 Hz, bandpassed from 1–40 Hz with an FIR filter of order 100 and epoched 0.1–1 second after each cursor movement. For more details about the experiment please refer to [36].

For the CSP-NN method, we used FIR filters of order 100 to filter the EEG data on each channel in 1–3, 2–5, 4–7, 6–10, 7–12, 10–15, 12–19, 18–25, 19–30, 25–35, and 30–40

Hz frequency bands to cover low and high theta, mu and beta bands while compensating for individual differences [36].

We randomly selected 5 divisions of train-validation-test sets in which right and left imagery classes were balanced in each set. Performance is reported as the average of the classification accuracy on the test sets.

5.5 Results and discussion

As the EEGNet architecture for ERD/ERS data outperforms deep ConvNet [99], we restrict comparison of our TA-CSPNN to shallow ConvNet and EEGNet. For dataset I, performance of TA-CSPNN with $F_t = 8$ temporal filters and $F_s = 2$ spatial filters is presented in Table 5.2 and is compared with EEGNet(8,2) [99] and shallow ConvNet (Sh-ConvNet) [98]. For this dataset, the length of the temporal kernel and the dropout parameter were set to $K = 63$ and $p = 0.25$ respectively for both EEGNet and TA-CSPNN. Shallow ConvNet was originally proposed for a sampling rate of 250 Hz. Since we downsampled the data by two, we also divided the lengths of the temporal kernels and pooling layers by two: temporal kernel length was set to 13, pool size in the average pooling layer to (1,35) with a stride of size (1,7) as suggested by [99].

For each participant, all models were trained on the train set with 10% for validation and tested on the evaluation set (as originally distributed for the purpose of the BCI competition). Performance is reported as the average of the classification accuracy on the evaluation set for a model trained with 10 different initializations. Shallow ConvNet performs significantly better than TA-CSPNN for A2 and A4 but does significantly worse for A1, A3, A8 and A9 (paired-sample t-test, $p < 0.05$). However, the difference between EEGNet and TA-CSPNN is not statistically significant (paired-sample t-test, $p > 0.1$).

Table 5.3 reports the length of EEG epochs (L), the sampling rate (SRate) and the number

of trainable parameters in each architecture for dataset I. Note that the number of parameters in TA-CSPNN is about half the number of parameters in EEGNet and less than 2.5% of the number of parameters in shallow ConvNet.

Table 5.2: Classification rates for dataset I. Note that this is a four-class classification.

PID	Sh-ConvNet	EEGNet(8,2)	TA-CSPNN(8,2)
A1	0.61	0.69	0.71
A2	0.39	0.40	0.36
A3	0.70	0.79	0.79
A4	0.55	0.49	0.44
A5	0.38	0.38	0.39
A6	0.42	0.46	0.44
A7	0.70	0.71	0.72
A8	0.62	0.73	0.72
A9	0.68	0.78	0.76

Table 5.3: Number of parameters for dataset I: trial length is 2 seconds at sampling rate of 125 Hz.

L	SRate	Sh-ConvNet	EEGNet(8,2)	TA-CSPNN(8,2)
2 s	125 Hz	40644	1900	972

For dataset II, the length of the temporal kernel and dropout parameter were set to $K = 50$ and $p = 0.25$ for both EEGNet and TA-CSPNN. Since CSP-NN has 11 temporal filters and 6 spatial filters (equivalent to the top three filters for each class in CSP), we set the number of temporal and spatial filters in both EEGNet and TA-CSPNN to $F_t = 11$ and $F_s = 6$ respectively.

CSP-NN was implemented slightly different than [21]: we used batch normalization [101] after the Conv2D layer for each frequency band and also used dropout with $p = 0.25$ after the squared-average pooling layer. Then the merged features from different frequency bands were passed to a dense layer with 30 hidden units and ELU activation function before the output layer.

Table 5.4: Classification rates for dataset II.

PID	CSP-NN	EEGNet(11,6)	TA-CSPNN(11,6)
P1	0.87	0.87	0.87
P2	0.66	0.68	0.74
P3	0.71	0.70	0.71
P4	0.74	0.78	0.76
P5	0.83	0.91	0.89
P6	0.74	0.68	0.74
P7	0.87	0.82	0.86
P8	0.82	0.77	0.88
P9	0.69	0.72	0.75
P10	0.71	0.67	0.78

Table 5.5: Number of parameters for dataset II: trial length is 0.9 seconds at sampling rate of 100 Hz.

L	SRate	CSP-NN	EEGNet(11,6)	TA-CSPNN(11,6)
0.9 s	100 Hz	6560	10738	5062

Table 5.4 reports the classification accuracy for each participant in dataset II. TA-CSPNN does significantly better than EEGNet (paired-sample t-test, $p < 0.05$) in P2, P6, P8 and P10. For the rest of the participants, the difference between EEGNet and TA-CSPNN is not statistically significant.

Table 5.5 reports the length of EEG epochs (L) for dataset II as well as the sampling rate (SRate) and the number of trainable parameters for each model applied to dataset II. Note that TA-CSPNN uses less than half the number of parameters in EEGNet.

5.6 Conclusions and future work

In this work, we proposed a temporally adaptive convolutional neural network-based implementation of the widely used FB-CSP to classify ERD/ERS: TA-CSPNN. Our model uses

about half the number of parameters in EEGNet [99] and less than 2.5% of that used by shallow ConvNet [98] and shows comparable or improved results for motor imagery classification on a publicly available dataset (BCI Competition IV, dataset 2a) and another motor imagery dataset [36].

Our proposed architecture is easily generalized to incorporate spatio-temporal features in each filter bank by changing the spatial convolution kernel size [21, 107]. Also, regularization methods that have been proposed to improve CSP [108] can be incorporated as regularization terms on the weights in the spatial convolution layer. Moreover, the hidden layers may provide additional useful feedback signals for online motor imagery training [84].

5.7 Acknowledgments

This work was supported by NSF IIS 1219200, IIS 1817226, SMA 1041755, and IIS 1528214, FISP G2171, G3155, NIH 5T32MH020002-18 and Mary Anne Fox dissertation year fellowship.

Chapter Acknowledgments

Chapter 5, in full, is a reprint of material as it appears in Mahta Mousavi, and Virginia R. de Sa. “Temporally adaptive common spatial patterns with deep convolutional neural networks,” 2019 41st Annual International Conference of the IEEE Engineering in Medicine and Biology Society (EMBC), Berlin, Germany, 2019, pp. 4533-4536, doi: 10.1109/EMBC.2019.8857423. The dissertation author was the primary author of this publication. The copyright for this publication is owned by IEEE and used in accordance with their terms and conditions.

Chapter 6

Spatio-temporal analysis of the error-related brain activity

6.1 Abstract

Electroencephalography (EEG)-based braincomputer interface (BCI) systems infer brain signals recorded via EEG without using common neuromuscular pathways. User brain response to BCI error is a contributor to non-stationarity of the EEG signal and poses challenges in developing reliable active BCI control. Many passive BCI implementations, on the other hand, have the detection of error-related brain activity as their primary goal. Therefore, reliable detection of this signal is crucial in both active and passive BCIs. In this work, we propose CREST: a novel covariance-based method that uses Riemannian and Euclidean geometry and combines spatial and temporal aspects of the feedback-related brain activity in response to BCI error. We evaluate our proposed method with two datasets: an active BCI for 1-D cursor control using motor imagery and a passive BCI for 2-D cursor control. We show significant improvement across participants in both datasets compared to existing methods.

6.2 Introduction

Brain-computer interface (BCI) systems record brain activity directly from the brain using methods such as electroencephalography (EEG) and attempt to infer the users intent [2, 23]. Active BCIs such as motor imagery (MI) BCIs are among common BCI systems in which the user imagines moving a part of her/his body resulting in a decrease in power (called an event-related desynchronization or ERD) in various frequency bands [8, 24]. Movement imagination of different body parts leads to spatially different desynchronization that can be used by the BCI to detect the imagined movement. In practice, the imagined movement classes (such as right/left hand) can be mapped to, for example, a switch, to control the movement of a robotic limb or a wheelchair. This BCI output is referred to as BCI feedback and the brain response to BCI feedback as feedback-related brain activity. One source of non-stationarity in EEG signals is the feedback-related brain activity [36]. Error-related potentials (ErrP) and error-related spectral components are among the components of this signal [36]. If not taken into account, these signals can pose challenges for real-world application of a BCI system [12, 10, 36]. In previous work, we have shown that when the feedback-related activity is appropriately modeled, the information can be combined with the motor imagery classification to greatly improve the overall BCI performance [36].

Separate work in passive BCIs (pBCI) [63, 109] has shown that the users intentions or emotional states can be detected through passive cognitive monitoring and that this signal can be used as an (implicit) control source [74, 110]. Therefore, in both active and passive BCIs, single-trial classification of the users state with respect to the BCI feedback (whether the BCI output is perceived as an error/undesired or not) is a critical component of a reliable BCI.

Previous work on classifying feedback-related brain activity varies by the type of features used and the classifier that is trained on these features [12]. For instance, authors in [10] and [54] focused on temporal features from one or two fronto-central channels, while others such as

[74] considered all available EEG channels and used a windowed-means approach as instructed by [90].

Riemannian geometry has been shown to be promising for reliable classification in various BCI paradigms [111, 22, 112, 113]. Methods based on Riemannian geometry have also been used for data augmentation to balance classes for error detection in a P300 speller task [114]. However, to our knowledge, there is no work in the literature that attempts to classify error-related or feedback-related brain activity using Riemannian methods.

In this paper, we explore ways to improve the classification of the error-related brain activity so as to further improve its contribution to an overall BCI system. Specifically, we investigate the spatio-temporal aspects of the error-related brain activity using covariance matrices in two different BCI paradigms by looking at both space and time covariances through Euclidean and Riemannian geometry. Our goal is to better distinguish whether the BCI feedback (output) is perceived by the user as an error.

We evaluate our proposed methods through two different datasets: one from our previous study in which participants were actively controlling cursor movements using right/left-hand motor imagery and another dataset shared with us by Zander and Krol et al. [74] in which participants were passively controlling a cursor on a screen in front of them. An earlier version of this work appeared in [115].

6.3 Data collection and pre-processing

6.3.1 Dataset I: active cursor control with motor imagery

Data were recorded from 10 participants after the study was approved by the University Institutional Review Board at UC San Diego. All participants signed a consent form prior to participating in the experiment. EEG data were recorded using a 64-channel BrainAmp system (Brain Products GmbH) at 5000 Hz. Channels were located according to the international 10–20

system and were referenced online to FCz.

Participants were instructed to use motor imagery of their right/left hand to control a cursor on a screen in front of them to the right/left toward a target [84]. At the beginning of each trial, the cursor and the target appeared at the center and three steps away from the center at either right or left side of the screen, respectively (see Figure 6.1). The cursor moved one step every second and trials ended when the cursor hit the target location or the other end of the screen. Participants believed that they were in control of the cursor movements; however, the cursor moved based on a pre-determined sequence of movements that was kept the same across participants. This was to have enough cursor movements toward/away from the target (i.e. good/bad movements) for each participant irrespective of the motor imagery performance. The cursor sequence of movement was randomly generated subject to a few constraints, e.g., no more than two consecutive changes in direction were allowed. For more details about the experiment, please refer to [36].

The overall goal in a motor-imagery BCI is to detect the imagined class. The common method is to train a classifier to distinguish between right-hand and left-hand motor imagery (or whatever imagery classes have been mapped to 'move cursor right' and 'move cursor left'). As shown in our earlier work [36], there is another classifiable aspect in the EEG signal – whether the cursor moved in the desired or non-desired direction. In the analysis for this paper, our goal is to improve this classification of whether the user was satisfied with the last cursor movement or not, i.e. if the cursor had just moved toward (good) or away (bad) from the target. We call this a good/bad (G/B) classifier.

6.3.2 Dataset II: passive cursor control

This dataset was recorded at the Technische Universität Berlin, Germany, from 19 participants and shared with us by Zander and Krol et al. [74]. All participants signed a consent form accepted by the ethics committee of the Department of Psychology and Ergonomics before

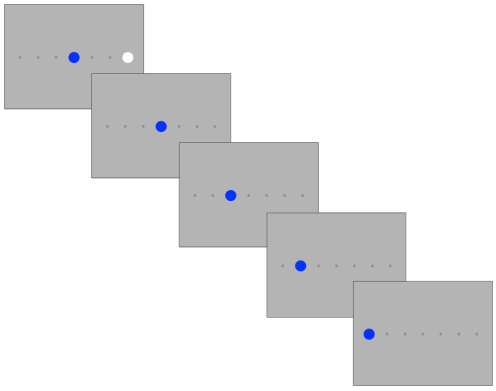

Figure 6.1: An example of a trial in dataset I. Participants were instructed to use right/left-hand motor imagery to move the cursor (the blue circle) to right/left toward the target (white circle). We considered movements toward/away from the target as good/bad movements perceived by the participants [36].

taking part in the experiment. Data were recorded using a 64-channel BrainAmp system (Brain Products GmbH) at 500 Hz. Channels were located according to the international 10–20 system and were referenced online to FCz.

This study had multiple parts including offline and online cursor control; however, we considered only the offline data that were used for calibration in the original study. This part of the study consisted of a cursor moving randomly on a 4×4 grid. Participants were instructed to observe cursor movements on the grid and evaluate each movement as 'appropriate' or 'inappropriate' with respect to reaching the target, which was located in one of the corners of the grid. The cursor moved randomly to one of up to eight adjacent nodes until it reached the target, after which another target was selected and the procedure restarted in the next trial. For more details about the experiment, please refer to [74].

Angular deviance from the optimal path was used to describe and categorize the movements. In Figure 6.2, the target is in the top right corner and the cursor (red) at the bottom row. A movement upwards (depicted in Figure 6.2b) has an angular deviance of 18°, whereas Figure 6.2c depicts an angular deviance of 63°. We considered angles that were below 45° as good movements and angles above 130° as bad movements and the EEG data corresponding to these two labels were used to train a good/bad (G/B) classifier. The angles in between were labeled as

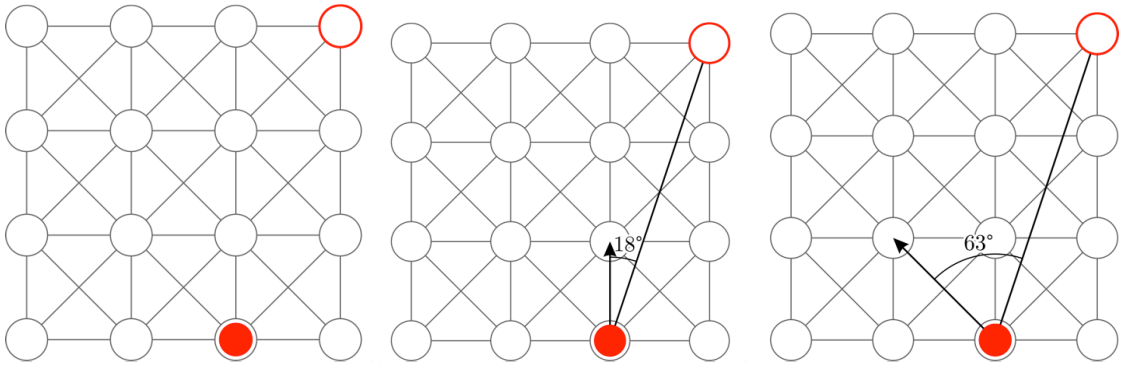

(a) (b) (c)

Figure 6.2: In dataset II, participants were instructed to 'judge' each cursor (red full circle) movement (indicated by the arrow in the static figure) as satisfactory or unsatisfactory with respect to its movement toward/away from the target (red empty circle) [74]. Diagram (a) depicts a cursors location and diagrams (b) and (c) specify different next cursor movements and how the angle between the cursor direction of movement and the direct line connecting the cursor to the target location is defined. We considered angles smaller than 45° as good movements and larger than 130° as bad movements perceived by the participants.

neutral and not used for classification.

6.3.3 Pre-processing

In each dataset, sections that were contaminated with excessive noise were removed. Independent component analysis (ICA) [66] was applied to data from each participant and independent components representing muscle and eye artifacts were removed. Pre-processing was done in MATLAB [37] and EEGLAB [38]. A maximum of 1 and 3 noisy channels were removed from datasets I and II, respectively. The removed channels were interpolated using EEGLAB and all 64 channels were used for feature extraction and classification. Data were re-referenced to the common average, downsampled to 100 Hz, and filtered in 0.5–10, 1–3, 2–5, 4–7, 6–10, 7–12, 10–15, 12–19, 18–25, 19–30, 25–35, 30–40 Hz with a 100th-order FIR filter using a Kaiser window. The first frequency band was used for the windowed-means method only as will be described in more detail later. Next, data were epoched 50–950 ms after each cursor movement and this segment is called a 'step' in what follows. Classification results are reported on a single

cursor movement, i.e. for every step.

6.4 Feature extraction and classification

Feature extraction and classification were implemented in Python. We used scikit-learn [93] to implement classifiers and the pyRiemann toolbox [116] to calculate Riemannian distances and means.

In each dataset, classes (good and bad) were balanced by randomly subsampling the larger class. Therefore, we generated 10 instances of train-test combinations which were kept the same across the different tested methods. In each instance, the train-test ratio is about 4:1. On average, in dataset I instances, there are 573 train and 142 test steps. In dataset II instances, the average train and test steps are 197 and 49, respectively.

Covariance matrices are used at the core of several feature extraction methods in BCI applications [19, 111, 117]. The methods discussed in this work use space and time covariances of the good (toward the target) and bad (away from the target) steps. Moreover, we looked at different frequency bands, namely 1–3, 2–5, 4–7, 6–10, 7–12, 10–15, 12–19, 18–25, 19–30, 25–35, 30–40 Hz covering the low and high theta, mu, and beta frequency bands and to cover for potential individual differences [36, 67]. Covariance matrices were calculated in each frequency band separately. Next, we will explain how we estimated covariances to capture spatial and temporal features and how these were used for classification.

6.4.1 Space and time covariances

Let p represent the number of channels, t the number of time samples and $i \in \{1, ..., N\}$ where N is the number of steps available. Let $X_i \in \mathbb{R}^{p \times t}$ be an EEG epoch (i.e. step) and C_{s_i} and C_{t_i} be the sample space and time covariances for the i^{th} step, respectively. Since the number of time samples in our case (i.e., 90 time samples at 100 Hz sampling rate) is larger than

the number of EEG channels $p = 64$, time covariances are not full rank and thus not positive definite. Also, as we removed eye and muscle components through ICA, space covariances are also rank deficient. Therefore, we used regularization to make the covariance matrices full-rank. Space and time covariances were regularized as follows:

$$C \leftarrow (1-\alpha)C + \alpha\frac{trace(C)}{N}I, \tag{6.1}$$

where C is the covariance matrix, α is the regularization parameter, $trace(C)$ is the sum of the diagonal elements of C and I is the identity matrix with the same size as C. We used a data driven method [118] to estimate the regularization parameter for data from each participant, in each frequency band for space and time covariances separately. We only used train data to estimate the shrinkage parameters (α).

6.4.2 Common spatial patterns (CSP)

The filter bank common spatial patterns (FB-CSP) algorithm was proposed by Ang et al. [20] to detect the imagined movement class in a motor imagery BCI. Inspired by this method, in our previous work, we used a similar approach to classify the error-related brain activity in a motor imagery BCI [36].

Let $C^g_{s_i}$ and $C^b_{s_i}$ represent the space covariance of the i^{th} good and bad steps, respectively, for a specific frequency band. The average of the trace normalized sample covariances for each of the good and bad classes were estimated as:

$$\Sigma_g = \frac{1}{N}\sum_i C^g_{s_i}/trace(C^g_{s_i}) \tag{6.2}$$

and

$$\Sigma_b = \frac{1}{N}\sum_i C^b_{s_i}/trace(C^b_{s_i}) \tag{6.3}$$

respectively, where N is the number of steps. As mentioned earlier, the number of steps in good and bad classes were balanced. CSP filters for each frequency band were estimated by simultaneous diagonalization of the two covariance matrices:

$$W^T \Sigma_g W = \Lambda^g \qquad W^T \Sigma_b W = \Lambda^b \tag{6.4}$$

where Λ^g and Λ^b are diagonal matrices such that $\Lambda^g + \Lambda^b = I$ [19]. CSP filters, represented by the columns of W, are the solutions of the following generalized eigenvalue problem:

$$\Sigma_g W = \lambda \Sigma_b W. \tag{6.5}$$

Next, 6 filters (eigenvectors) corresponding to the 3 largest and smallest eigenvalues were selected. EEG epochs were filtered through the selected filters in each frequency band. The logarithm of the variance (across time) of the filtered EEG data through each of the 6 selected filters were calculated as features. These 6 features in each of the 11 frequency bands were used for classification using a 66D regularized linear discriminant analysis (r-LDA) classifier [93, 119, 19].

6.4.3 Common temporal patterns (CTP)

The common temporal patterns (CTP) algorithm, proposed by Yu et al. [120], is the temporal counterpart of the common spatial patterns in which the sample mean of the good and bad time covariances are considered instead of space covariances. Similar to FB-CSP, we consider a filter bank version of CTP. EEG epochs were filtered through 6 CTP filters (corresponding to the 3 largest and smallest eigenvalues) in each frequency band and the logarithm of the variance (across 64 channels) of the filtered epochs were selected as features (6 features for each band, hence a total of 66 features). A regularized linear discriminant analysis (r-LDA) was trained on

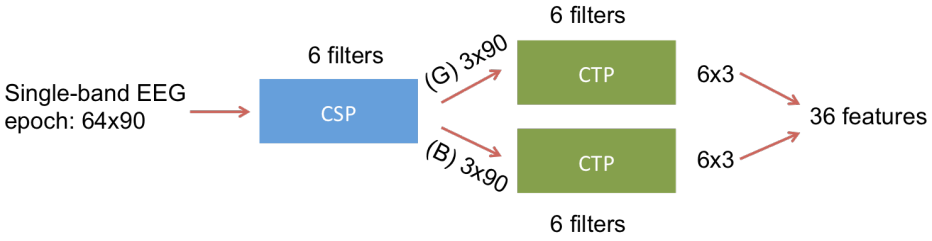

Figure 6.3: Method of CSP-CTP: CSP filters are trained on each frequency band ($p = 64$ and $t = 90$). Six CSP filters (corresponding to the 3 largest and smallest eigenvalues) are selected and EEG epochs are filtered through each. Then, CTP filters are trained on the good (G) and bad (B) CSP-filtered data separately.

the selected features [93, 119].

6.4.4 Common spatial and temporal patterns (CSP-CTP)

To combine spatio-temporal features, we first calculated CSP filters and selected 6 filters (corresponding to the 3 largest and smallest eigenvalues). Then, EEG epochs were filtered through the CSP filters corresponding to the good class. The CTP method was then used to capture temporal features by learning 6 CTP filters (corresponding to the 3 largest and smallest eigenvalues). Another set of 6 CTP filters were trained using the EEG epochs filtered through the CSP filters corresponding to the bad class. Figure 6.3 describes this method.

The above procedure was done in each frequency band separately to select a total of 36 features and the selected features from all 11 frequency bands were concatenated. Finally, a regularized-LDA classifier was trained [93, 119].

6.4.5 Distance to Riemannian mean of spatial covariances (DRM-S)

Full-rank covariance matrices lie on a Riemannian manifold pertaining to the symmetric positive definite (SPD) matrices [111]. Let $A(n)$ be the set of all $n \times n$ SPD matrices. The

Riemannian distance between $A_1 \in A(n)$ and $A_2 \in A(n)$ is defined as follows:

$$\delta_R(A_1, A_2) = ||Log(A_1^{-1}A_2)||_F = [\sum_{i=1}^{n} log^2 \lambda_i]^{1/2} \tag{6.6}$$

where λ_i are the eigenvalues of $(A_1^{-1}A_2)$. Since A_1 and A_2 are both SPD, λ_i are real positive (non-zero) values. Also, $||.||_F$ represents the Frobenius norm and $Log(.)$ the matrix logarithm.

The mean of the SPD matrices $A_1, A_2, ..., A_l$ on the Riemannian manifold is defined as follows [111]:

$$M(A_1, A_2, ..., A_l) = argmin_{X \in A(n)} \sum_{i=1}^{l} \delta_R^2(X, A_i). \tag{6.7}$$

There is no closed form solution for (6.7); however, it can be solved iteratively [121].

Based on the defined matrix relationships on the manifold, we propose a filter bank generalization of the minimum distance to Riemannian mean (MDM) classifier [116]. First, the Riemannian mean of the good and bad space covariances in each frequency band on the training set were estimated as described earlier. Next, in each frequency band, features were selected as the Riemannian distances to the Riemannian means of the good and bad classes. This resulted in a total of 22 features: 11 frequency bands $\times$ 2 good and bad classes. A logistic regression classifier was trained on the selected features [93]. We trained a logistic regression classifier for all Riemannian methods since we found that the distribution of features was far from a multivariate normal distribution.

6.4.6 Distance to Riemannian mean of temporal covariances (DRM-T)

This method is the temporal counterpart of the DRM-S method described previously. After the Riemannian mean of the good and bad time covariances in each frequency band on the training set were estimated, features were selected as the Riemannian distances to the Riemannian means of the good and bad classes. This resulted in a total of 22 features: 11 frequency bands $\times$ 2 good and bad classes. Logistic regression was trained on the selected features [93].

6.4.7 Distance to Riemannian mean of spatial and temporal covariances (DRM-ST)

This method combines spatial and temporal Riemannian geometry-based features by concatenating DRM-S and DRM-T features described in the previous two subsections. This resulted in a total of 44 features: 11 frequency bands $\times$ 2 good and bad classes $\times$ 2 time and space covariances. A logistic regression classifier was trained on the selected features [93].

6.4.8 Covariance-based Riemannian and Euclidean spatio-temporal classifier (CREST)

We combined DRM-ST and CSP-CTP to capture spatiotemporal features using both Riemannian and common spatial and temporal classifiers. We call this method CREST. For each classifier, we first calculated the signed distance of each trial to the decision hyperplane and applied a logistic function to estimate the probability of the trial belonging to the the good (or bad) class as the classifier score. Logistic regression was used to combine DRM-ST and CSP-CTP classifier scores [93].

6.4.9 Windowed-means (WM)

We compared our proposed methods with the windowed means method which is widely used for single-trial event-related potential (ERP) classification [90, 74]. EEG data on each channel were bandpass filtered to 0.5–10 Hz as described earlier and epoched 50–950 ms after each cursor movement. We calculated the mean of the signal on each channel in 9 non-overlapping time windows, i.e. each covering 100 ms. Then, a regularized linear discriminant analysis (r-LDA) classifier was trained on the selected features [93, 119, 90].

6.4.10 CREST+WM

Finally, we combined DRM-ST, CSP-CTP and WM as well to compare with the WM classifier to determine whether WM and CREST capture different features. Logistic regression was used to combine DRM-ST, CSP-CTP and WM classifier scores as explained earlier [93].

6.5 Results and discussion

Figures 6.4 and 6.5 plot the event-related potential (ERP), i.e. the average EEG waveform time-locked to the cursor movement, for 'Good' and 'Bad' classes on channel Fz across participants for datasets I and II, respectively. For the plot, EEG data for each participant were high-pass filtered at 1 Hz and epoched 100 to 1000 ms time locked to each cursor movement. Then, the average waveform for each participant was calculated in each class. The solid lines on each plot represent the average across participants and the shaded color represents the standard error of the mean. Note that the two classes correspond to cursor movements toward/away from the target and our goal in this paper is to train a classifier to reliably distinguish among them after every cursor movement.

We compared the G/B classification performance in datasets I and II using CSP and DRM-S as well as CTP and DRM-T. Tables 6.1 and 6.2 report the average (first number in each entry) and standard error of the mean (second number in each entry) for classification accuracy over 10 instances of train-test for each participant in datasets I and II, respectively. On average, Riemannian methods perform better across participants and this difference is statistically significant for dataset I (paired-sample t-test, $p < 0.03$). DRM-T performs significantly better than CTP in dataset II (paired-sample t-test, $p < 0.01$). However, in this dataset, the difference between DRM-S and CSP is not statistically significant across participants.

Tables 6.3 and 6.4 report the classification accuracy of the windowed-means method (WM) and our proposed spatio-temporal methods: DRM-ST and CSP-CTP, CREST and

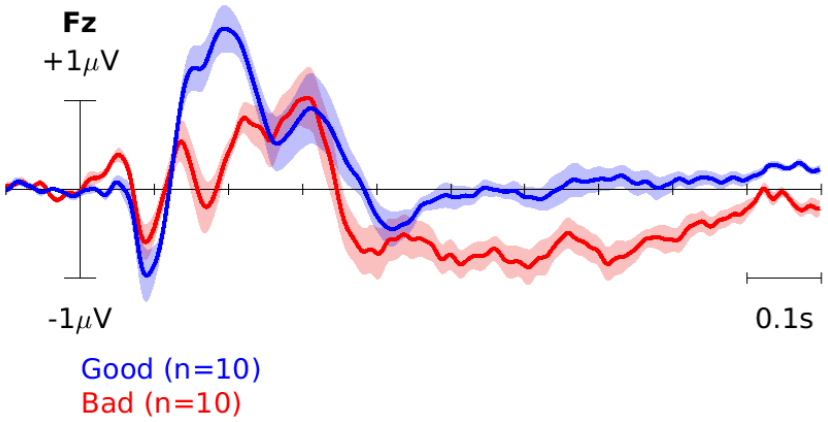

Figure 6.4: ERP in dataset I. The blue curve corresponds to the brain response to 'good' cursor movements, i.e. toward the target. The red curve, on the other hand, corresponds to the brain response to 'bad' movements, i.e. away from the target.

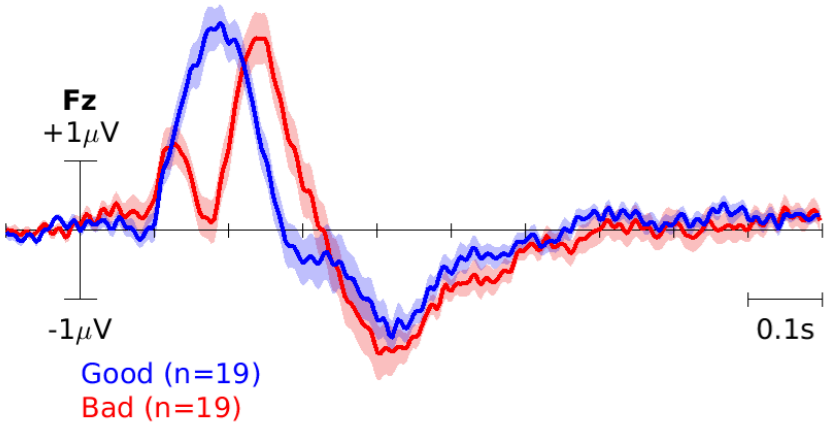

Figure 6.5: ERP in dataset II. The blue curve corresponds to the brain response to 'good' cursor movements, i.e. toward the target. The red curve, on the other hand, corresponds to the brain response to 'bad' movements, i.e. away from the target.

Table 6.1: Dataset I: G/B classification accuracy using spatial and temporal features separately. Each table entry is the average classification accuracy (first number) together with the standard error of the mean (second number) over 10 instances of train-test for each participant. Riemannian methods outperform their counterparts and this difference is significant across participants (paired-sample t-test, $p < 0.03$).

ID	CSP	DRM-S	CTP	DRM-T
A1	0.77/0.009	0.77/0.009	0.65/0.012	0.72/0.013
A2	0.74/0.017	0.74/0.011	0.64/0.015	0.68/0.014
A3	0.58/0.006	0.62/0.012	0.52/0.008	0.56/0.014
A4	0.74/0.007	0.76/0.010	0.63/0.011	0.64/0.011
A5	0.67/0.008	0.67/0.011	0.56/0.009	0.59/0.014
A6	0.73/0.006	0.72/0.010	0.62/0.011	0.68/0.014
A7	0.76/0.008	0.77/0.009	0.61/0.010	0.66/0.010
A8	0.66/0.016	0.71/0.009	0.66/0.013	0.71/0.007
A9	0.75/0.009	0.81/0.012	0.65/0.009	0.72/0.011
A10	0.67/0.016	0.71/0.015	0.66/0.012	0.69/0.012
Average	0.71/0.019	**0.73/0.017**	0.62/0.014	**0.67/0.016**

CREST+WM. We used paired-sample t-tests to compare the difference between WM and the other methods across participants for each dataset. CREST and CREST+WM outperform WM in both datasets (paired-sample t-test, $p < 0.006$, which stays significant at the 0.05 threshold with Bonferroni correction for the number of tests).

The difference in performance of DRM-ST and WM is not statistically significant for either of the datasets. However, CSP-CTP outperforms WM in dataset II and this difference is statistically significant (paired-sample t-test, $p < 0.005$, which stays significant at the 0.05 threshold with Bonferroni correction for the number of tests), while the performance of CSP-CTP in dataset I is not statistically different from that of WM.

Figures 6.6 and 6.7 show WM, CREST and CREST+WM performance as bar plots for easier visualization.

Table 6.2: Dataset II: G/B classification accuracy using spatial and temporal features separately. Each table entry is the average classification accuracy (first number) together with the standard error of the mean (second number) over 10 instances of train-test for each participant. DRM-T outperforms its counterpart and this difference is significant across participants (paired-sample t-test, $p < 0.01$). However, the difference between CSP and DRM-S is not statistically significant.

ID	CSP	DRM-S	CTP	DRM-T
P1	0.76/0.015	0.74/0.010	0.57/0.017	0.61/0.012
P2	0.64/0.018	0.65/0.015	0.61/0.016	0.67/0.015
P3	0.87/0.016	0.83/0.013	0.72/0.014	0.74/0.014
P4	0.65/0.026	0.73/0.023	0.62/0.021	0.71/0.016
P5	0.67/0.019	0.62/0.026	0.53/0.023	0.63/0.024
P6	0.63/0.027	0.62/0.018	0.54/0.019	0.53/0.022
P7	0.72/0.017	0.68/0.022	0.54/0.017	0.52/0.017
P8	0.84/0.017	0.80/0.012	0.52/0.019	0.62/0.024
P9	0.58/0.024	0.58/0.020	0.50/0.027	0.46/0.025
P10	0.54/0.027	0.58/0.018	0.55/0.017	0.61/0.019
P11	0.71/0.020	0.73/0.025	0.66/0.023	0.73/0.022
P12	0.64/0.023	0.69/0.014	0.59/0.017	0.62/0.023
P13	0.57/0.016	0.57/0.025	0.52/0.018	0.56/0.015
P14	0.60/0.017	0.62/0.023	0.58/0.016	0.56/0.016
P15	0.66/0.025	0.66/0.025	0.61/0.016	0.60/0.021
P16	0.77/0.016	0.71/0.026	0.63/0.010	0.64/0.011
P17	0.65/0.024	0.68/0.015	0.57/0.032	0.62/0.024
P18	0.59/0.018	0.64/0.023	0.60/0.030	0.55/0.027
P19	0.64/0.021	0.70/0.016	0.60/0.011	0.64/0.013
Average	0.67/0.021	0.68/0.016	0.58/0.012	**0.61/0.016**

Table 6.3: Dataset I: G/B classification accuracy comparing the proposed spatio-temporal methods and WM. Each table entry is the average classification accuracy (first number) together with the standard error of the mean (second number) over 10 instances of train-test for each participant. Significantly improved results across participants are represented in bold fonts (paired-sample t-test, $p < 0.006$, which stays significant at the 0.05 threshold with Bonferroni correction for the number of tests, i.e. 4).

ID	WM	DRM-ST	CSP-CTP	CREST	CREST+WM
A1	0.75/0.006	0.79/0.009	0.80/0.009	0.82/0.005	0.83/0.006
A2	0.79/0.010	0.77/0.012	0.76/0.007	0.82/0.007	0.85/0.007
A3	0.68/0.010	0.60/0.016	0.61/0.011	0.63/0.008	0.68/0.010
A4	0.83/0.011	0.77/0.014	0.88/0.011	0.91/0.007	0.90/0.009
A5	0.73/0.011	0.67/0.011	0.77/0.008	0.79/0.008	0.80/0.012
A6	0.72/0.009	0.74/0.015	0.69/0.008	0.76/0.004	0.78/0.005
A7	0.79/0.011	0.77/0.008	0.76/0.009	0.81/0.007	0.84/0.008
A8	0.69/0.014	0.72/0.005	0.71/0.012	0.76/0.011	0.77/0.014
A9	0.75/0.008	0.81/0.010	0.73/0.010	0.82/0.006	0.84/0.010
A10	0.74/0.014	0.73/0.016	0.75/0.009	0.78/0.007	0.80/0.009
Average	0.75/0.015	0.74/0.019	0.75/0.023	**0.79/0.022**	**0.81/0.019**

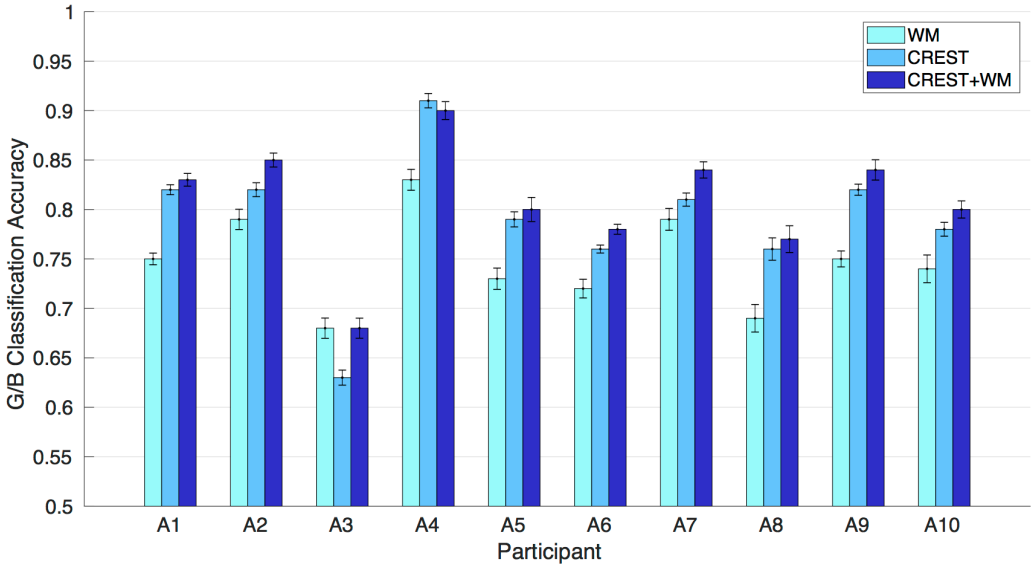

Figure 6.6: WM, CREST and CREST+WM in dataset I. The bars and error bars represent the average classification accuracy and the standard error of the mean, respectively, i.e. first and second entries in Table 6.3 columns 2, 5 and 6.

Table 6.4: Dataset II: G/B classification accuracy comparing the proposed spatio-temporal methods and WM. Each table entry is the average classification accuracy (first number) together with the standard error of the mean (second number) over 10 instances of train-test for each participant. Significantly improved results across participants are represented in bold fonts (paired-sample t-test, $p < 0.005$, which stays significant at the 0.05 threshold with Bonferroni correction for the number of tests, i.e. 4).

ID	WM	DRM-ST	CSP-CTP	CREST	CREST+WM
P1	0.77/0.008	0.72/0.019	0.83/0.017	0.84/0.012	0.81/0.013
P2	0.74/0.019	0.70/0.008	0.77/0.016	0.77/0.020	0.75/0.014
P3	0.84/0.021	0.83/0.011	0.90/0.013	0.90/0.010	0.89/0.016
P4	0.77/0.010	0.75/0.031	0.73/0.021	0.76/0.022	0.80/0.017
P5	0.70/0.020	0.66/0.025	0.79/0.018	0.79/0.017	0.78/0.022
P6	0.68/0.021	0.60/0.010	0.69/0.026	0.70/0.024	0.72/0.023
P7	0.72/0.017	0.67/0.011	0.73/0.017	0.73/0.012	0.76/0.014
P8	0.83/0.014	0.79/0.016	0.92/0.014	0.92/0.017	0.88/0.016
P9	0.58/0.023	0.54/0.025	0.64/0.024	0.65/0.023	0.63/0.024
P10	0.51/0.021	0.62/0.022	0.58/0.021	0.63/0.019	0.57/0.023
P11	0.77/0.017	0.76/0.021	0.78/0.017	0.79/0.023	0.84/0.018
P12	0.69/0.021	0.68/0.024	0.77/0.011	0.73/0.022	0.74/0.016
P13	0.59/0.015	0.58/0.013	0.72/0.024	0.71/0.023	0.66/0.010
P14	0.70/0.005	0.61/0.019	0.68/0.019	0.69/0.016	0.71/0.015
P15	0.68/0.016	0.66/0.019	0.67/0.024	0.70/0.020	0.73/0.016
P16	0.80/0.010	0.70/0.019	0.80/0.020	0.81/0.022	0.82/0.012
P17	0.80/0.009	0.68/0.021	0.77/0.025	0.77/0.020	0.82/0.019
P18	0.71/0.027	0.63/0.028	0.72/0.017	0.69/0.023	0.72/0.025
P19	0.57/0.026	0.71/0.021	0.73/0.009	0.74/0.017	0.73/0.016
Average	0.71/0.021	0.68/0.017	**0.75/0.019**	**0.75/0.018**	**0.76/0.019**

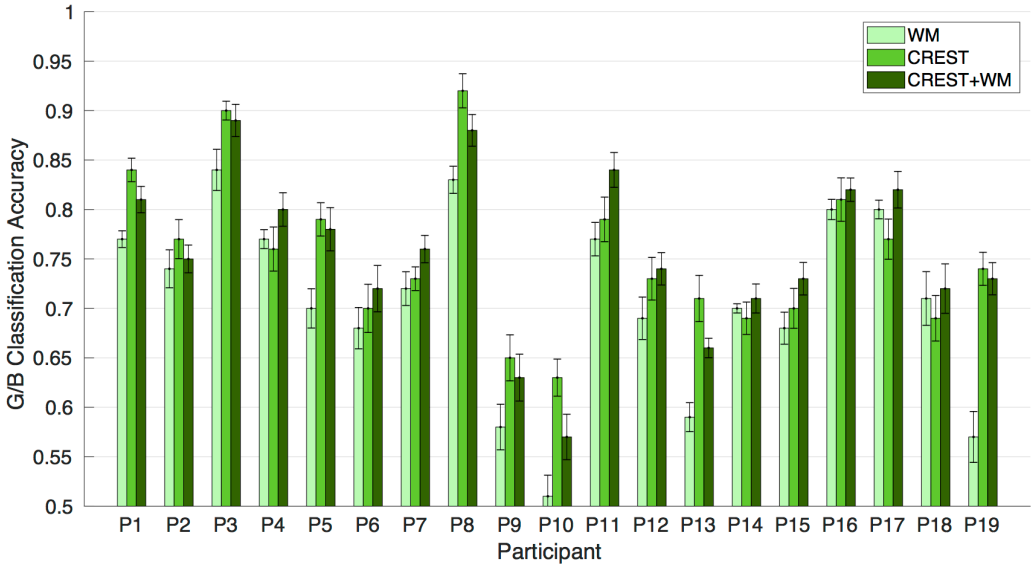

Figure 6.7: WM, CREST and CREST+WM in dataset II. The bars and error bars represent the average classification accuracy and the standard error of the mean, respectively, i.e. the first and second entries in Table 6.4 columns 2, 5 and 6.

6.6 Conclusions

We proposed spatio-temporal methods to classify the error-related brain activity and evaluated our results on two different datasets. The first dataset is from an active motor imagery BCI in which the users brain response to the BCI feedback is an implicit piece of information and using this information can improve the overall BCI performance [36]. We also evaluated our proposed methods on a passive BCI dataset in which participants were evaluating the movements of a cursor. In the latter, error-related brain activity is the core information to be classified even though it is not explicitly provided by the user.

We compared DRM-S and DRM-T that use Riemannian distances as features, with CSP and CTP methods, respectively, in their capacity for classifying feedback-related brain activity in response to BCI error. Our results show that on average across participants in both datasets, methods that use features from Riemannian geometry are more powerful when considering spatial or temporal features separately.

We also proposed methods to combine spatial and temporal features that use Riemannian distances (DRMST) and Euclidean geometry-based methods of common patterns (CSP-CTP). We also proposed to combine these two methods (CREST) and showed that this combined method outperforms the windowed-means (WM) method and the difference is statistically significant across participants in both datasets.

6.7 Acknowledgments

We would like to thank Laurens R. Krol and Thorsten O. Zander for sharing their dataset with us.

This work was supported by the NSF [IIS 1219200, 1817226, 1528214]; DAAD [short-term research grant]; UC San Diego [Chancellors Research Innovation Scholarships G2171, G3155 and the Mary Anne Fox dissertation year fellowship]; NIH [5T32MH020002-18].

Chapter Acknowledgments

Chapter 6, in full is a reprint of material as it appears in Mahta Mousavi, and Virginia R. de Sa. "Spatio-temporal analysis of error-related brain activity in active and passive brain-computer interfaces," Brain-Computer Interfaces, 2019, doi: 10.1080/2326263X.2019.1671040. The dissertation author was the primary author of this publication.

Chapter 7

Summary and future directions

A brain-computer interface (BCI) is a collaboration between a user and a computer towards a certain goal. In motor imagery BCI systems, the user should be able to generate brain activity that is recognizable by the computer. The computer on the other hand, should be able to learn the relevant underlying features of the user's brain activity to best classify it and provide a reliable control command (feedback/output). As many existing BCI systems are limited to the laboratory environment, this dissertation addresses existing issues through various studies. In this chapter, we briefly summarize our findings and elaborate on the future directions that they inspire.

Training participants to perform motor imagery is known to be a difficult task. We investigated the current state-of-the-art training protocols and proposed a more elaborate feedback to give participants a better chance to learn how to generate discriminable motor imagery signal (Chapter 2). We showed that over the course of a session, the proposed feedback allowed participants to gain a better control of their motor imagery signal. Nevertheless, it remains to investigate whether the proposed elaborated feedback paradigm allows the BCI users to perform better across multiple sessions and how the learned skills last over time compared to existing methods. This can be done with a multiple session study.

We also investigated the effect of feedback on brain activity signals and proposed a novel motor imagery BCI that will use the error-related brain activity to improve the overall BCI performance (Chapter 3). Furthermore, we showed the performance of our proposed method in a real-time motor imagery BCI control. Our results showed that the proposed hybrid BCI that incorporates the error-related brain activity into the BCI design performs significantly better than a conventional motor imagery system (Chapter 4). We showed that the error-related brain activity is more reliable than the motor imagery signal. Since error-related brain activity exists in other BCI paradigms as well – in both active and passive BCI systems – it is important to investigate its application in further improving other BCI paradigms. More specifically, it is interesting to investigate the differences of the error-related brain activity across different BCI systems, among different sessions for the same user or even among different users [95]. Another interesting direction will be to investigate the use of adaptive classifiers for both the R/L and G/B classifiers to further improve the proposed BCI system.

We further investigated the applicability of more sophisticated machine learning approaches to better capture spatio-temporal aspects of motor imagery and error-related brain activity. For the former, we proposed a convolutional neural network-based architecture that utilizes fewer trainable parameters compared to existing architectures and yet performs similarly or better. We showed our results on two different motor imagery datasets (Chapter 5). Our proposed method (TA-CSPNN) provides an end-to-end feature extraction and classification framework to classify the motor imagery signal. We have also shown that a CSP-based classifier can capture the relevant features for the error-related brain activity (Chapters 3 and 4). One interesting future work is to use a similar architecture to classify the error-related brain activity and to combine it with the motor imagery signal. Also, investigating the transfer of a trained model among different users is another direction that can be pursued.

As for the spatio-temporal aspects of the error-related brain activity, we proposed CREST: a novel covariance-based method that uses Riemannian and Euclidean geometry and

combines spatial and temporal aspects of the error-related brain activity. We showed the efficacy of our proposed method in comparison to existing methods in classification of the error-related brain activity in an active motor imagery BCI for a 1-D cursor control and in a passive BCI for a 2-D cursor control (Chapter 6). Given the computational complexity of the Riemannian geometry framework, it is important to investigate how it can be incorporated in a real-time application especially with shorter calibration times (i.e., limited training data).

Through a novel training paradigm, along with better utilization of the available brain signals and finally a novel BCI design that captures the user brain response to BCI output (feedback), this dissertation vastly improves the performance (classification accuracy and hit rates) and reliability (consistency from calibration to online use) of motor imagery based brain-computer interfaces. As such, it provides the potential to greatly increase the number of people who are successfully able to operate one. Moreover, the developed techniques could be useful for discovering and training other mental commands that could be used in EEG-based BCIs not limited to motor imagery BCIs.

References

[1] Jacques J Vidal. Toward direct brain-computer communication. *Annual review of Biophysics and Bioengineering*, 2(1):157–180, 1973.

[2] Lawrence Ashley Farwell and Emanuel Donchin. Talking off the top of your head: toward a mental prosthesis utilizing event-related brain potentials. *Electroencephalography and clinical Neurophysiology*, 70(6):510–523, 1988.

[3] Gert Pfurtscheller and Christa Neuper. Motor imagery and direct brain-computer communication. *Proceedings of the IEEE*, 89(7):1123–1134, 2001.

[4] Luis Fernando Nicolas-Alonso and Jaime Gomez-Gil. Brain computer interfaces, a review. *sensors*, 12(2):1211–1279, 2012.

[5] Maria A Cervera, Surjo R Soekadar, Junichi Ushiba, José del R Millán, Meigen Liu, Niels Birbaumer, and Gangadhar Garipelli. Brain-computer interfaces for post-stroke motor rehabilitation: a meta-analysis. *Annals of clinical and translational neurology*, 5(5):651–663, 2018.

[6] Efthymios Angelakis, Stamatina Stathopoulou, Jennifer L Frymiare, Deborah L Green, Joel F Lubar, and John Kounios. EEG neurofeedback: a brief overview and an example of peak alpha frequency training for cognitive enhancement in the elderly. *The clinical neuropsychologist*, 21(1):110–129, 2007.

[7] Ricardo Chavarriaga, Melanie Fried-Oken, Sonja Kleih, Fabien Lotte, and Reinhold Scherer. Heading for new shores! overcoming pitfalls in BCI design. *Brain-Computer Interfaces*, 4(1-2):60–73, 2017.

[8] Gert Pfurtscheller, Clemens Brunner, Alois Schlögl, and FH Lopes Da Silva. Mu rhythm (de) synchronization and EEG single-trial classification of different motor imagery tasks. *NeuroImage*, 31(1):153–159, 2006.

[9] Fabien Lotte, Florian Larrue, and Christian Mühl. Flaws in current human training protocols for spontaneous brain-computer interfaces: lessons learned from instructional design. *Frontiers in human neuroscience*, 7:568, 2013.

[10] Gerwin Schalk, Jonathan R Wolpaw, Dennis J McFarland, and Gert Pfurtscheller. EEG-based communication: presence of an error potential. *Clinical neurophysiology*, 111(12):2138–2144, 2000.

[11] Pierre W Ferrez and José del R Millán. Simultaneous real-time detection of motor imagery and error-related potentials for improved BCI accuracy. In *Proceedings of the 4th international brain-computer interface workshop and training course*, number CNBI-CONF-2008-004, pages 197–202, 2008.

[12] Ricardo Chavarriaga, Aleksander Sobolewski, and José del R Millán. Errare machinale est: the use of error-related potentials in brain-machine interfaces. *Frontiers in neuroscience*, 8:208, 2014.

[13] Martin Spüler, Michael Bensch, Sonja Kleih, Wolfgang Rosenstiel, Martin Bogdan, and Andrea Kübler. Online use of error-related potentials in healthy users and people with severe motor impairment increases performance of a P300-BCI. *Clinical Neurophysiology*, 123(7):1328–1337, 2012.

[14] Ricardo Chavarriaga and José del R Millán. Learning from EEG error-related potentials in noninvasive brain-computer interfaces. *IEEE transactions on neural systems and rehabilitation engineering*, 18(4):381–388, 2010.

[15] Xavier Artusi, Imran Khan Niazi, Marie-Françoise Lucas, and Dario Farina. Performance of a simulated adaptive BCI based on experimental classification of movement-related and error potentials. *IEEE Journal on Emerging and Selected Topics in Circuits and Systems*, 1(4):480–488, 2011.

[16] Martin Spüler, Wolfgang Rosenstiel, and Martin Bogdan. Online adaptation of a c-VEP brain-computer interface (BCI) based on error-related potentials and unsupervised learning. *PloS one*, 7(12):e51077, 2012.

[17] Adam S. Koerner and Virginia R. de Sa. A novel method to integrate error detection into motor imagery BCI. In *Workshop on Brain-Machine body interfaces, 34th Annual International Conference of the IEEE Engineering in Medicine and Biology Society*. IEEE, 2012.

[18] Adam S. Koerner. *Investigating natural control signals for brain-computer interfaces*. PhD thesis, UC San Diego, 2013.

[19] Benjamin Blankertz, Ryota Tomioka, Steven Lemm, Motoaki Kawanabe, and K-R Muller. Optimizing spatial filters for robust EEG single-trial analysis. *IEEE Signal processing magazine*, 25(1):41–56, 2008.

[20] Kai Keng Ang, Zheng Yang Chin, Chuanchu Wang, Cuntai Guan, and Haihong Zhang. Filter bank common spatial pattern algorithm on BCI competition IV datasets 2a and 2b. *Frontiers in neuroscience*, 6:39, 2012.

[21] Daniel Maryanovsky, Mahta Mousavi, Nathanial G Moreno, and Virginia R de Sa. CSP-NN: A convolutional neural network implementation of common spatial patterns. In *Proceedings of the 7th Graz Brain-Computer Interface Conference 2017*, pages 302–307, 2017.

[22] Marco Congedo, Alexandre Barachant, and Rajendra Bhatia. Riemannian geometry for EEG-based brain-computer interfaces; a primer and a review. *Brain-Computer Interfaces*, 4(3):155–174, 2017.

[23] Jonathan R Wolpaw, Dennis J McFarland, Gregory W Neat, and Catherine A Forneris. An EEG-based brain-computer interface for cursor control. *Electroencephalography and clinical neurophysiology*, 78(3):252–259, 1991.

[24] Dennis J McFarland, Laurie A Miner, Theresa M Vaughan, and Jonathan R Wolpaw. Mu and beta rhythm topographies during motor imagery and actual movements. *Brain topography*, 12(3):177–186, 2000.

[25] Jaime A Pineda, Brendan Z Allison, and Andrey Vankov. The effects of self-movement, observation, and imagination on/spl mu/rhythms and readiness potentials (RP's): toward a brain-computer interface (BCI). *IEEE Transactions on Rehabilitation Engineering*, 8(2):219–222, 2000.

[26] Han-Jeong Hwang, Kiwoon Kwon, and Chang-Hwang Im. Neurofeedback-based motor imagery training for brain–computer interface (BCI). *Journal of neuroscience methods*, 179(1):150–156, 2009.

[27] Jonathan Mercier-Ganady, Fabien Lotte, Emilie Loup-Escande, Maud Marchal, and Anatole Lécuyer. The mind-mirror: See your brain in action in your head using EEG and augmented reality. In *2014 IEEE Virtual Reality (VR)*, pages 33–38. IEEE, 2014.

[28] Jérémy Frey, Renaud Gervais, Stéphanie Fleck, Fabien Lotte, and Martin Hachet. Teegi: tangible EEG interface. In *Proceedings of the 27th annual ACM symposium on User interface software and technology*, pages 301–308. ACM, 2014.

[29] Christa Neuper and Gert Pfurtscheller. Neurofeedback training for BCI control. In *Brain-computer interfaces*, pages 65–78. Springer, 2009.

[30] Tobias Kaufmann, John Williamson, E Hammer, R Murray-Smith, and A Kübler. Visually multimodal vs. classic unimodal feedback approach for SMR-BCIs: a comparison study. *Int. J. Bioelectromagn*, 13:80–81, 2011.

[31] Josef Faller, Carmen Vidaurre, Teodoro Solis-Escalante, Christa Neuper, and Reinhold Scherer. Autocalibration and recurrent adaptation: Towards a plug and play online ERD-BCI. *IEEE Transactions on Neural Systems and Rehabilitation Engineering*, 20(3):313–319, 2012.

[32] Camille Jeunet, Alison Cellard, Sriram Subramanian, Martin Hachet, Bernard N'Kaoua, and Fabien Lotte. How well can we learn with standard BCI training approaches? a pilot study. 2014.

[33] Valerie J Shute. Focus on formative feedback. *Review of educational research*, 78(1):153–189, 2008.

[34] UC San Diego Swartz Center for Computational Neuroscience. Simulation and Neuroscience Application Platform (SNAP). https://github.com/sccn/SNAP .

[35] Dennis J. McFarland, Lynn M. McCane, Stephen V. David, and Jonathan R. Wolpaw. Spatial filter selection for EEG-based communication. *Electroencephalography and Clinical Neurophysiology*, 103(3):386–394, 1997.

[36] Mahta Mousavi, Adam S Koerner, Qiong Zhang, Eunho Noh, and Virginia R de Sa. Improving motor imagery BCI with user response to feedback. *Brain-Computer Interfaces*, 4(1-2):74–86, 2017.

[37] MATLAB and Statistics Toolbox Release 2015a. The MathWorks Inc., Natick, Massachusetts, United States, 2015.

[38] Arnaud Delorme and Scott Makeig. EEGLAB: an open source toolbox for analysis of single-trial EEG dynamics including independent component analysis. *J Neuroscience Methods*, 134(1):9–21, 2004.

[39] Benjamin Blankertz, Gabriel Curio, and Klaus-Robert Müller. Classifying single trial EEG: Towards brain computer interfacing. In T. G. Dietterich, S. Becker, and Z. Ghahramani, editors, *Advances in Neural Information Processing Systems 14*, pages 157–164. MIT Press, 2002.

[40] Tim Mullen. Cleanline EEGLAB plugin. *Neuroimaging Informatics Toolsand Resources Clearinghouse (NITRC)*, 2012.

[41] Jason A Palmer, Ken Kreutz-Delgado, and Scott Makeig. AMICA: An adaptive mixture of independent component analyzers with shared components. *Swartz Center for Computatonal Neursoscience, University of California San Diego, Tech. Rep*, 2012.

[42] Gernot Müller-Putz, Reinhold Scherer, Clemens Brunner, Robert Leeb, and Gert Pfurtscheller. Better than random: a closer look on bci results. *International Journal of Bioelectromagnetism*, 10(ARTICLE):52–55, 2008.

[43] Joachim Kalcher, Doris Flotzinger, Ch Neuper, Silvia Gölly, and Gert Pfurtscheller. Graz brain-computer interface II: towards communication between humans and computers based on online classification of three different EEG patterns. *Medical and biological engineering and computing*, 34(5):382–388, 1996.

[44] José del R Millán, Rüdiger Rupp, Gernot Mueller-Putz, Roderick Murray-Smith, Claudio Giugliemma, Michael Tangermann, Carmen Vidaurre, Febo Cincotti, Andrea Kubler, Robert Leeb, et al. Combining brain–computer interfaces and assistive technologies: state-of-the-art and challenges. *Frontiers in neuroscience*, 4:161, 2010.

[45] Steven G Mason, Ali Bashashati, Mehrdad Fatourechi, Karla F Navarro, and Gary E Birch. A comprehensive survey of brain interface technology designs. *Annals of biomedical engineering*, 35(2):137–169, 2007.

[46] Josef Faller. BCIs that use steady-state visual evoked potentials or slow cortical potentials. In *Brain-Computer Interfaces, Principles and Practice*. Oxford University Press, 2012.

[47] Eeic W Sellers, Yael Arbel, and Emanuel Donchin. 12 BCIs that use P300 event-related potentials. *Brain-computer interfaces: principles and practice*, 2012.

[48] Paul S. Hammon. *Adaptive online brain-computer interface for interpretation and visualization of desired reach*. PhD thesis, UC San Diego, 2009.

[49] Christa Neuper, Reinhold Scherer, Selina Wriessnegger, and Gert Pfurtscheller. Motor imagery and action observation: modulation of sensorimotor brain rhythms during mental control of a brain–computer interface. *Clinical neurophysiology*, 120(2):239–247, 2009.

[50] Kai Keng Ang and Cuntai Guan. Brain-computer interface in stroke rehabilitation. *Journal of Computer Science and Engineering*, 7(2):139–146, 2013.

[51] Adam S. Koerner, Qiong Zhang, and Virginia R. de Sa. The effect of real-time positive and negative feedback on motor imagery performance. In *the International BCI Meeting*, 2013.

[52] Sam Darvishi, Michael C Ridding, Derek Abbott, and Mathias Baumert. Does feedback modality affect performance of brain computer interfaces? In *2015 7th International IEEE/EMBS Conference on Neural Engineering (NER)*, pages 232–235. IEEE, 2015.

[53] Jaromir Doležal, Vladimír Černỳ, and Jakub Štastnỳ. Online motor-imagery based BCI. In *2012 International Conference on Applied Electronics*, pages 65–68. IEEE, 2012.

[54] Pierre W Ferrez and José del R Millán. Error-related EEG potentials generated during simulated brain–computer interaction. *IEEE transactions on biomedical engineering*, 55(3):923–929, 2008.

[55] Xavier Artusi, Imran Khan Niazi, Marie-Françoise Lucas, and Dario Farina. Accuracy of a BCI based on movement-related and error potentials. In *2011 Annual International Conference of the IEEE Engineering in Medicine and Biology Society*, pages 3688–3691. IEEE, 2011.

[56] Nico M. Schmidt, Benjamin Blankertz, and Matthias S. Treder. Online detection of error-related potentials boosts the performance of mental typewriters. *BMC Neuroscience*, 13(1):19, 2012.

[57] Alex Kreilinger, Christa Neuper, and Gernot R. Müller-Putz. Error potential detection during continuous movement of an artificial arm controlled by brain–computer interface. *Medical & Biological Engineering & Computing*, 50(3):223–230, 2012.

[58] Jason Omedes, Inaki Iturrate, Luis Montesano, and Javier Minguez. Using frequency-domain features for the generalization of EEG error-related potentials among different tasks. In *2013 35th Annual International Conference of the IEEE Engineering in Medicine and Biology Society (EMBC)*, pages 5263–5266. IEEE, 2013.

[59] Tomislav Milekovic, Tonio Ball, Andreas Schulze-Bonhage, Ad Aertsen, and Carsten Mehring. Error-related electrocorticographic activity in humans during continuous movements. *Journal of neural engineering*, 9(2):026007, 2012.

[60] Jijun Tong, Qinguang Lin, Ran Xiao, and Lei Ding. Combining multiple features for error detection and its application in brain–computer interface. *Biomedical engineering online*, 15(1):17, 2016.

[61] Scott Makeig. Auditory event-related dynamics of the EEG spectrum and effects of exposure to tones. *Electroencephalography and clinical neurophysiology*, 86(4):283–293, 1993.

[62] Thorsten O Zander, Christian Kothe, Sabine Jatzev, and Matti Gaertner. Enhancing human-computer interaction with input from active and passive brain-computer interfaces. In *Brain-computer interfaces*, pages 181–199. Springer, 2010.

[63] Thorsten O Zander and Christian Kothe. Towards passive brain–computer interfaces: applying brain–computer interface technology to human–machine systems in general. *Journal of neural engineering*, 8(2):025005, 2011.

[64] Christa Neuper, Reinhold Scherer, Miriam Reiner, and Gert Pfurtscheller. Imagery of motor actions: Differential effects of kinesthetic and visual? motor mode of imagery in single-trial EEG. *Cognitive Brain Research*, 25(3):668–677, 2005.

[65] George H Klem, Hans Otto Lüders, HH Jasper, C Elger, et al. The ten-twenty electrode system of the international federation. *Electroencephalogr Clin Neurophysiol*, 52(3):3–6, 1999.

[66] Scott Makeig, Anthony J Bell, Tzyy-Ping Jung, and Terrence J Sejnowski. Independent component analysis of electroencephalographic data. In *Advances in neural information processing systems*, pages 145–151, 1996.

[67] Eunho Noh, Grit Herzmann, Tim Curran, and Virginia R de Sa. Using single-trial EEG to predict and analyze subsequent memory. *NeuroImage*, 84:712–723, 2014.

[68] Fabien Lotte, Marco Congedo, Anatole Lécuyer, Fabrice Lamarche, and Bruno Arnaldi. A review of classification algorithms for EEG-based brain–computer interfaces. *Journal of neural engineering*, 4(2):R1, 2007.

[69] Martin Spüler and Christian Niethammer. Error-related potentials during continuous feedback: using EEG to detect errors of different type and severity. *Frontiers in human neuroscience*, 9:155, 2015.

[70] Noman Naseer and Keum-Shik Hong. Classification of functional near-infrared spectroscopy signals corresponding to the right-and left-wrist motor imagery for development of a brain–computer interface. *Neuroscience letters*, 553:84–89, 2013.

[71] Keum-Shik Hong, Noman Naseer, and Yun-Hee Kim. Classification of prefrontal and motor cortex signals for three-class fNIRS-BCI. *Neuroscience letters*, 587:87–92, 2015.

[72] Joshua M Stivers, Laurens R Krol, Virginia R de Sa, and Thorsten O Zander. Spelling with cursor movements modified by implicit user response. In *Proceedings of the 6th International Brain-Computer Interface Meeting*, page 28, 2016.

[73] Timothy Zeyl, Erwei Yin, Michelle Keightley, and Tom Chau. Improving bit rate in an auditory BCI: Exploiting error-related potentials. *Brain-Computer Interfaces*, 3(2):75–87, 2016.

[74] Thorsten O Zander, Laurens R Krol, Niels P Birbaumer, and Klaus Gramann. Neuroadaptive technology enables implicit cursor control based on medial prefrontal cortex activity. *Proceedings of the National Academy of Sciences*, 113(52):14898–14903, 2016.

[75] Virginia R. de Sa. An interactive control strategy is more robust to non-optimal classification boundaries. In *Proceedings of the 14th ACM International Conference on Multimodal Interaction*, ICMI '12, pages 579–586, New York, NY, USA, 2012. ACM.

[76] Virginia R de Sa. Changing the commands in noisy incremental human controlled systems. In *NIPS Workshop*, 2014.

[77] Eric W Sellers, Theresa M Vaughan, and Jonathan R Wolpaw. A brain-computer interface for long-term independent home use. *Amyotrophic lateral sclerosis*, 11(5):449–455, 2010.

[78] Elisa Mira Holz, Loic Botrel, Tobias Kaufmann, and Andrea Kübler. Long-term independent brain-computer interface home use improves quality of life of a patient in the locked-in state: a case study. *Archives of physical medicine and rehabilitation*, 96(3):S16–S26, 2015.

[79] Pradeep Shenoy, Matthias Krauledat, Benjamin Blankertz, Rajesh PN Rao, and Klaus-Robert Müller. Towards adaptive classification for BCI. *Journal of neural engineering*, 3(1):R13, 2006.

[80] Lucas C Parra, Clay D Spence, Adam D Gerson, and Paul Sajda. Response error correction-a demonstration of improved human-machine performance using real-time EEG monitoring. *IEEE transactions on neural systems and rehabilitation engineering*, 11(2):173–177, 2003.

[81] Tomislav Milekovic, Tonio Ball, Andreas Schulze-Bonhage, Ad Aertsen, and Carsten Mehring. Detection of error related neuronal responses recorded by electrocorticography in humans during continuous movements. *PloS one*, 8(2):e55235, 2013.

[82] Nile R Wilson, Devapratim Sarma, Jeremiah D Wander, Kurt E Weaver, Jeffrey G Ojemann, and Rajesh PN Rao. Cortical topography of error-related high-frequency potentials during erroneous control in a continuous control brain–computer interface. *Frontiers in neuroscience*, 13, 2019.

[83] Nir Even-Chen, Sergey D Stavisky, Jonathan C Kao, Stephen I Ryu, and Krishna V Shenoy. Augmenting intracortical brain-machine interface with neurally driven error detectors. *Journal of neural engineering*, 14(6):066007, 2017.

[84] Mahta Mousavi and Virginia R de Sa. Towards elaborated feedback for training motor imagery brain computer interfaces. In *Proceedings of the 7th Graz Brain-Computer Interface Conference 2017*, pages 332–337, 2017.

[85] Richard C Oldfield. The assessment and analysis of handedness: the Edinburgh inventory. *Neuropsychologia*, 9(1):97–113, 1971.

[86] Oliver P John, Sanjay Srivastava, et al. The Big Five trait taxonomy: History, measurement, and theoretical perspectives. *Handbook of personality: Theory and research*, 2(1999):102–138, 1999.

[87] Julian B Rotter. Generalized expectancies for internal versus external control of reinforcement. *Psychological monographs: General and applied*, 80(1):1, 1966.

[88] Michael F Scheier, Charles S Carver, and Michael W Bridges. Distinguishing optimism from neuroticism (and trait anxiety, self-mastery, and self-esteem): a reevaluation of the Life Orientation Test. *Journal of personality and social psychology*, 67(6):1063, 1994.

[89] Eric Jones, Travis Oliphant, Pearu Peterson, et al. Scipy: Open source scientific tools for Python. 2001.

[90] Benjamin Blankertz, Steven Lemm, Matthias Treder, Stefan Haufe, and Klaus-Robert Müller. Single-trial analysis and classification of ERP components – a tutorial. *NeuroImage*, 56(2):814–825, 2011.

[91] UC San Diego Swartz Center for Computational Neuroscience. Lab Streaming Layer (LSL). `https://github.com/sccn/labstreaminglayer` .

[92] Travis E Oliphant. *A guide to NumPy*, volume 1. Trelgol Publishing USA, 2006.

[93] Fabian Pedregosa, Gaël Varoquaux, Alexandre Gramfort, Vincent Michel, Bertrand Thirion, Olivier Grisel, Mathieu Blondel, Peter Prettenhofer, Ron Weiss, Vincent Dubourg, et al. Scikit-learn: Machine learning in Python. *Journal of machine learning research*, 12(Oct):2825–2830, 2011.

[94] MATLAB and Statistics Toolbox Release 2018b. The MathWorks Inc., Natick, Massachusetts, United States, 2018.

[95] Mohammad Abu-Alqumsan, Christoph Kapeller, Christoph Hintermüller, Christoph Guger, and Angelika Peer. Invariance and variability in interaction error-related potentials and their consequences for classification. *Journal of neural engineering*, 14(6):066015, 2017.

[96] Herbert Ramoser, Johannes Muller-Gerking, and Gert Pfurtscheller. Optimal spatial filtering of single trial EEG during imagined hand movement. *IEEE transactions on rehabilitation engineering*, 8(4):441–446, 2000.

[97] Alex Krizhevsky, Ilya Sutskever, and Geoffrey E Hinton. ImageNet classification with deep convolutional neural networks. In *Advances in neural information processing systems*, pages 1097–1105, 2012.

[98] Robin Tibor Schirrmeister, Jost Tobias Springenberg, Lukas Dominique Josef Fiederer, Martin Glasstetter, Katharina Eggensperger, Michael Tangermann, Frank Hutter, Wolfram Burgard, and Tonio Ball. Deep learning with convolutional neural networks for EEG decoding and visualization. *Human brain mapping*, 38(11):5391–5420, 2017.

[99] Vernon Lawhern, Amelia Solon, Nicholas Waytowich, Stephen M Gordon, Chou Hung, and Brent J Lance. EEGNet: a compact convolutional neural network for EEG-based brain–computer interfaces. *Journal of neural engineering*, 2018.

[100] Nitish Srivastava, Geoffrey Hinton, Alex Krizhevsky, Ilya Sutskever, and Ruslan Salakhutdinov. Dropout: a simple way to prevent neural networks from overfitting. *The Journal of Machine Learning Research*, 15(1):1929–1958, 2014.

[101] Sergey Ioffe and Christian Szegedy. Batch normalization: Accelerating deep network training by reducing internal covariate shift. *arXiv preprint arXiv:1502.03167*, 2015.

[102] François Chollet et al. Keras. `https://keras.io` , 2015.

[103] Martín Abadi et al. TensorFlow: Large-scale machine learning on heterogeneous systems, 2015. Software available from tensorflow.org.

[104] Diederik P Kingma and Jimmy Ba. Adam: A method for stochastic optimization. *arXiv preprint arXiv:1412.6980*, 2014.

[105] Rich Caruana, Steve Lawrence, and C Lee Giles. Overfitting in neural nets: Backpropagation, conjugate gradient, and early stopping. In *Advances in neural information processing systems*, pages 402–408, 2001.

[106] Clemens Brunner, Robert Leeb, Gernot Müller-Putz, Alios Schlögl, and Gert Pfurtscheller. BCI competition 2008–Graz data set A. *Institute for Knowledge Discovery (Laboratory of Brain-Computer Interfaces), Graz University of Technology*, 16, 2008.

[107] Dean J Krusienski, Eric W Sellers, and Theresa M. Vaughan. Common spatio-temporal patterns for the P300 speller. In *Neural Engineering, 2007. CNE'07. 3rd International IEEE/EMBS Conference on*, pages 421–424. IEEE, 2007.

[108] Fabien Lotte and Cuntai Guan. Regularizing common spatial patterns to improve BCI designs: unified theory and new algorithms. *IEEE Transactions on biomedical Engineering*, 58(2):355–362, 2011.

[109] Laurens R Krol, Lena M Andreessen, and Thorsten O Zander. Passive brain-computer interfaces: A perspective on increased interactivity. *Brain-Computer Interfaces Handbook: Technological and Theoretical Advances*, pages 69–86, 2018.

[110] Thorsten O Zander, Jonas Brönstrup, Romy Lorenz, and Laurens R Krol. Towards BCI-based implicit control in human–computer interaction. In *Advances in Physiological Computing*, pages 67–90. Springer, 2014.

[111] Alexandre Barachant, Stéphane Bonnet, Marco Congedo, and Christian Jutten. Riemannian geometry applied to BCI classification. In *International Conference on Latent Variable Analysis and Signal Separation*, pages 629–636. Springer, 2010.

[112] Emmanuel K Kalunga, Sylvain Chevallier, Quentin Barthélemy, Karim Djouani, Eric Monacelli, and Yskandar Hamam. Online SSVEP-based BCI using Riemannian geometry. *Neurocomputing*, 191:55–68, 2016.

[113] Alexandre Barachant and Marco Congedo. A plug&play P300 BCI using information geometry. *arXiv preprint arXiv:1409.0107*, 2014.

[114] Emmanuel K Kalunga, Sylvain Chevallier, and Quentin Barthélemy. Data augmentation in Riemannian space for brain-computer interfaces. In *STAMLINS*, 2015.

[115] Mahta Mousavi and Virginia R de Sa. Spatio-temporal analysis of feedback-related brain activity in brain-computer interfaces. *NeurIPS 2018 Workshop on modeling and decision-making in the spatiotemporal domain*, 2018.

[116] Alexandre Barachant, Stéphane Bonnet, Marco Congedo, and Christian Jutten. Multiclass brain–computer interface classification by Riemannian geometry. *IEEE Transactions on Biomedical Engineering*, 59(4):920–928, 2012.

[117] Fabien Lotte, Laurent Bougrain, Andrzej Cichocki, Maureen Clerc, Marco Congedo, Alain Rakotomamonjy, and Florian Yger. A review of classification algorithms for EEG-based brain–computer interfaces: a 10 year update. *Journal of neural engineering*, 15(3):031005, 2018.

[118] Juliane Schäfer and Korbinian Strimmer. A shrinkage approach to large-scale covariance matrix estimation and implications for functional genomics. *Statistical applications in genetics and molecular biology*, 4(1), 2005.

[119] Olivier Ledoit and Michael Wolf. Improved estimation of the covariance matrix of stock returns with an application to portfolio selection. *Journal of empirical finance*, 10(5):603–621, 2003.

[120] Ke Yu, Kaiquan Shen, Shiyun Shao, Wu Chun Ng, Kenneth Kwok, and Xiaoping Li. Common spatio-temporal pattern for single-trial detection of event-related potential in rapid serial visual presentation triage. *IEEE Transactions on Biomedical Engineering*, 58(9):2513–2520, 2011.

[121] Maher Moakher. A differential geometric approach to the geometric mean of symmetric positive-definite matrices. *SIAM Journal on Matrix Analysis and Applications*, 26(3):735–747, 2005.